

Constraining Dark Matter through the spin temperature

Jouke Jensma

ABSTRACT

We investigate the influence of several decaying and annihilating dark matter candidates on the 21-cm spin temperature and on the thermal history of the Universe. These DM particles among others include sterile neutrinos and neutralinos. Their effect on the 21-cm background radiation field will be investigated. Properties of the dark matter candidates are taken from the literature and their effect on the background radiation field will be calculated.

Contents

Contents	1
1 Introduction	2
2 The physics	4
2.1 Hydrogen atom hyperfine structure	4
2.2 Spin temperature	5
2.3 The Wouthuysen-Field effect	5
2.4 Atomic collisions	7
2.5 Dark matter decay / annihilation	7
2.6 Fractional energy absorbed by the IGM	9
2.7 Determining kinetic temperature evolution	10
2.8 The background radiation arising from DM decay/annihilations	11
2.9 Relevant quantities	12
2.9.1 Sterile neutrinos	12
2.9.2 Neutralinos	12
2.9.3 Light Dark Matter	12
2.9.4 Exciting Dark Matter	13
2.9.5 Minimal Dark Matter	13
2.10 Constraining DM through the 21-cm background	13
3 Results	15
4 Summary & discussion	21
Bibliography	23
5 Appendix	25
5.1 Figures with $dn/dE = E^{-1}$	25
5.2 Figures with a mono-energetic energy spectrum	27
5.3 Other energy spectra	30
5.4 Differential brightness temperatures	31
5.5 Absorbed fractions	31

1. Introduction

Long ago, around a redshift of ≥ 1100 the Universe was unlike the Universe we currently reside in. At this time, before recombination, it was filled with ionized plasma, a giant soup of unbound particles. As the Universe continued to expand, the radiation field energy density and temperature dropped and the free electrons and protons grew cold enough to be able to recombine into atomic hydrogen and helium. With recombination the mean free path of photons became larger than the Hubble radius and the Universe became transparent. It is these photons we see today as the Cosmic Microwave Background (CMB).

After recombination the Universe becomes very simple as nothing much happens, that is except that the initial density fluctuations, seeded at the inflationary epoch, grow slowly through gravitational instability. At some stage these fluctuations become so nonlinear that they allow the formation of the first structures in the Universe at about $z = 20$. Once the first luminous sources emerged at $z \sim 10$ the reionization of the Universe began. The exact redshift at which reionization started is still unknown. However, we know that by $z = 6.5$ the Universe is already ionized as the spectra of the Sloan Digital Sky Survey (SDSS) high redshift quasars indicate (Fan et al., 2003, 2006). Moreover, the CMB data measured by the Wilkinson Microwave Anisotropy Probe (WMAP) satellite gives the optical depth for Thomson scattering up to recombination suggesting that reionization happened at $z < 10$ for any reasonable reionization history.

The timeframe between redshifts ~ 6.5 and ~ 1100 is one of the frontiers of cosmology due to the huge gap in the available data. The CMB provides us with information about the primordial density fluctuations of the Universe at that time, whereas galaxy/quasar surveys provide information about the Universe at $z \leq 6.5$. In that period the primordial density fluctuations that we observe on the CMB managed to set the stage for the formation of the large scale structure of the Universe. The details of what happened in the roughly 800 million years in between are largely unknown.

Due to the expansion of the Universe, particle number densities drop as $(1+z)^3$. This has a profound effect on the thermal and ionization history of the Universe. The residual free electrons in existence interact with baryons, coupling the gas temperature to the CMB temperature. However, as the energy density of the CMB photon field (and thus that of the residual free electrons which were coupled with the CMB photons), the ionized fraction and the densities continued to drop with the expansion of the Universe, it lost its temperature coupling with the matter. This happened around a redshift of about 200. With nothing left in place to heat the matter, it shifted to a higher adiabat and started to cool down as $(1+z)^2$ instead of $(1+z)$.

As the first luminous sources emerged at $z \sim 20$, they start to ionize and heat the surrounding Intergalactic Medium (IGM). After a sufficient number of these sources form the number of ionizing photons per baryon in the Universe is large enough for the ionization bubbles around individual sources to become volume filling (Madau et al., 1997).

The reionization scenario discussed so far has mainly to do with the baryons and first objects. However, at redshift higher than 10 there is another possible player in this story, the dark matter (DM). With DM composing over 80% of the matter content in the Universe, the question arises: could it not have any effect on the thermal and ionization history of the Universe?

DM is still a mysterious entity in astronomy. There are indications that it exists and that it is predominantly cold, obtained through several independent probes, including the distribution of galaxies on the sky, the observed cluster properties, the observed rotation curves of galaxies and many others. In particular, standard cosmological models also require the existence of DM in order to fit the WMAP data. Therefore, the question is what properties the DM particles have. Properties of DM (like mass-mixing angle relationships for neutrinos, mass-energy itself, lifetimes and others) have been constrained by several authors (see Boehm et al. (2004); Hooper and Wang (2004); Ascasibar et al. (2006); Bertone et al. (2005); Dolgov and Hansen (2002) and many others). Non-detection of

signals has also put hard constraints on DM properties and its interaction with baryonic matter (see Watson et al. (2006); Boyarsky et al. (2006); Abazajian et al. (2001) and many others).

In this report we will consider Weakly Interacting Massive Particle (WIMP) DM candidates, which is one of the most studied DM types. Mainly, we investigate the influence of possible DM decay/annihilation products (hereafter called DM products) on the heating, ionization and excitation of the IGM. These products can be photons, electrons, positrons or even other exotic particles. In particular, we study the effect of the DM products interaction with the IGM on the 21-cm spin temperature of neutral hydrogen relative to the standard case (without DM products). We show that this interaction can in some cases leave a small imprint on the 21-cm background signal. If observed, this would allow us to constrain the DM properties better, hence narrowing down the number of DM candidates, with future high redshift 21-cm observations.

In radio astronomy one observes the brightness temperature of the 21-cm radiation which, in the optically thin case, is directly related to the spin temperature. The differential brightness temperature is the power received from the sky relative to some reference point (in this case it is the CMB temperature). More specifically, the differential brightness temperature is proportional to the difference between the 21-cm spin temperature and the CMB temperature. When the spin temperature exceeds the CMB temperature, the 21-cm radiation will be visible in emission. If the spin temperature is lower than the CMB temperature, the radiation will be visible in absorption. For higher redshifts, the CMB temperature is coupled to the kinetic (i.e., gas) temperature, rendering the 21-cm radiation with respect to the CMB at that time unobservable. However, as the IGM loses its coupling with the CMB (below $z \sim 200$) the gas cools down adiabatically as $(1+z)^2$. Because atomic collisions at redshift range 50-200 are efficient in coupling the spin temperature to the kinetic temperature, the IGM will be visible in absorption. With decreasing redshifts and decreasing densities, collisions become less important and as a result the spin temperature is coupled back to the CMB temperature at about $z = 30$.

The amplitude of the deviation is expected to be on the order of ~ 10 -100 mK. New radio telescopes (like LOFAR, 21CMA, MWA, SKA) currently under development are expected to reach this level of sensitivity for redshifts in the range of 6-11.5. Through the obtained data on the 21-cm background from these new telescopes we will be potentially able to constrain the DM candidates by their absorption or emission on the 21-cm background.

The amplitude of absorption or emission depends on DM properties like mass-energy, cross section, lifetime, etc. Once the new generation of radio telescopes is able to look out to high redshifts we may be able to determine what properties the DM in our Universe has through the time evolution pattern it imprints on the brightness temperature. These have a direct influence on the produced 21-cm signal.

In this report we derive the influence of the DM products on the IGM during the redshift range of 10–1100. This latter part is important because our equations are only valid for neutral IGM. At lower redshifts reionization has already begun, increasing the ionization fraction, so our assumptions do not hold which makes our results not applicable in this regime. That is why we limit ourselves to $z > 10$. The impact of DM products on the thermal evolution of the Universe, on Lyman- α (Ly- α) pumping and on atomic collisions and on the 21-cm spin temperature will be investigated. Ly- α pumping and atomic collisions are the physical processes responsible for driving the spin temperature towards the kinetic temperature of the IGM, enhancing the 21-cm signal. This will be explained in more detail in this report.

Several authors, including Valdés et al. (2007), Mapelli et al. (2006), Ripamonti et al. (2007) (hereafter called RMF), Ciardi and Madau (2003), have calculated the possible effects on the IGM at high redshifts. Doing this requires an accurate description of the physical processes that take place in transferring energy from the DM decay and annihilation products into the IGM. They have found that most DM products have some influence, but it is rather small. Our research covers the same points as theirs but uses a slightly different approach. Ripamonti et al. (2007) assume that DM has a mono-energetic spectrum. We drop the mono-energeticity assumption in our research and take a broader DM product energy spectrum. For comparison with other authors' results we will also compute the effects of a mono-energetic spectrum on the spin temperature and the observed signal.

Our results differ considerably from other authors' results. This difference is the most profound for the case where DM products are entirely made up of photons. For a photon to ionize, excite or heat the IGM it needs to interact with it first. For the Ripamonti et al. (2007) mono-energetic spectrum there is one high-energy photon which is less likely to get absorbed by the IGM than many lower-energy photons corresponding to our energy spectrum, which is essentially the key difference between our approaches. The reason a high-energy photon is less likely to hit the IGM is because of the photo-ionization cross section, which drops rapidly for increasing energy. Therefore, the overall absorption probability naturally increases for an energy spectrum because we have comparatively more low-energy photons, increasing the effects our DM products have on heating, ionizing and exciting the IGM. The fraction of energy deposited into the IGM for an energy spectrum is larger than for the high-energy one-photon case.

Because more energy is deposited, more energy will be put into heating and more atoms will be excited or ionized. This will have its influence on the thermal and ionization history of the Universe, possibly modifying it in a significant way. The kinetic temperature of the gas will increase. More ionizations will deposit more energy as heat into the IGM through secondary heating by the electrons, increasing the influence of collisions. This increased pumping rate will modify the 21-cm background signal from the standard case and from the Ripamonti et al. (2007) case.

This report is structured as follows: Section 2 covers the background physics, where the physical concepts of spin temperature, kinetic temperature evolution will be explained, and the absorbed energy fractions into the IGM will be derived and coupling mechanisms will be discussed. Section 3 has several figures of ionized fractions, absorbed fractions and spin temperatures. In section 4 differences between our results and those of other authors will be discussed. Lastly, we conclude in 4 with the conclusions.

2. The physics

2.1. Hydrogen atom hyperfine structure

We will discuss the origin of the 21-cm radiation in this section. A partial model of the hyperfine structure of the hydrogen atom will be presented to give the reader an understanding of the physics that gives rise to this radiation.

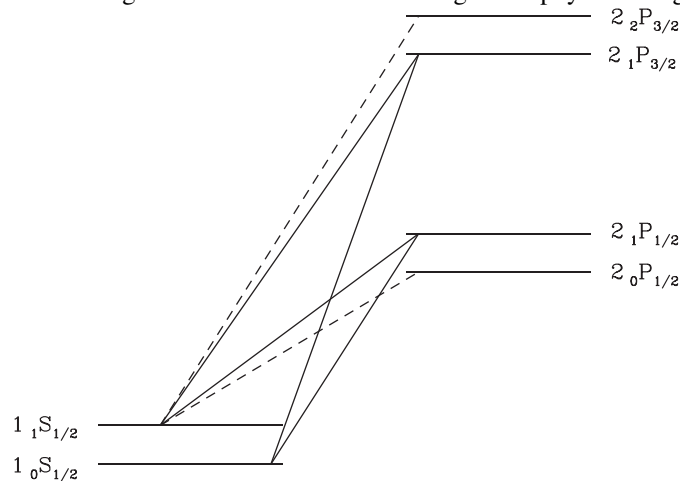


Fig. 1: Image adopted from Field (1958)

Figure (1) shows the partial hyperfine level structure of the hydrogen atom. The horizontal solid lines denote the hyperfine energy levels. These energy levels exist because of spin-spin interaction of the proton and the electron. For our purposes, the $1_1S_{1/2}$ and $1_0S_{1/2}$ levels are the most important, because an electron decaying from the excited hyperfine state to the ground hyperfine state emits 21-cm radiation. The other levels are displayed because they play a role in putting electrons into the excited hyperfine state. The dashed lines in the figure are transitions which are not important for our purposes because they have no influence on putting electrons in the hyperfine

excited state. However, the solid lines are allowed and they denote the possible transitions an electron can undergo while being excited from the ground hyperfine state to the excited hyperfine state.

The selection rules do not allow for an electron in $1_1S_{1/2}$ to decay to $1_0S_{1/2}$. However, there is a small probability that this transition does occur through a spontaneous spin flip of the electron. The mean lifetime of the excited state is $2.85 \times 10^{-15} \text{ s}^{-1}$. For the $1_1S_{1/2}$ state, the electron spin and proton spin are parallel (triplet state) whereas they are antiparallel for the $1_0S_{1/2}$ case (singlet state). The energy of the triplet state is slightly higher than the energy of the singlet state. This transition gives rise to the famous 21-cm line and it is only because there is so much neutral hydrogen in the Universe that we see this radiation in astrophysical systems.

2.2. Spin temperature

Any spin temperature referred to in this report refers to the 21-cm spin temperature. The physical definition is

$$\frac{n_1}{n_0} = \frac{g_1}{g_0} \exp\left(-\frac{T_*}{T_s}\right) \quad (1)$$

where $\frac{g_1}{g_0} = 3$. The g_0, g_1 are the weights of the singlet and triplet hyperfine levels with F quantum numbers 0 and 1. $T_* = \frac{h\nu_{10}}{k} = 0.0681 \text{ K}$ (where the latter equality only holds for the 21-cm line and k is the Boltzmann constant, ν_{10} is the frequency of the 1, 0 transition). The n_1, n_0 correspond to the $1_1S_{1/2}$ and $1_0S_{1/2}$ states and represent the number densities of electrons in the respective levels. The quantum number differing in these levels is that of the electron spin. Changing it will change the energy level the electron is in. Essentially, the spin temperature determines the ratio of the number densities of electrons in the two energy levels.

Ly- α pumping and collisions are processes capable of changing these number densities, thus changing the spin temperature in the process. This will be explained in more detail in the following sections.

Examining the limits for T_s we see that for $T_s \gg 1$ there are three times as many electrons in the upper energy level (compared to the lower energy level) as an upper limit, while for $T_s \ll 1$ all electrons sit in the lowest energy level. This is the electron distribution averaged over many hydrogen atoms. Only electrons decaying from the 1 to 0 quantum state can emit 21-cm radiation.

In his paper, Field (1958) has defined the spin temperature as

$$T_s = \frac{T_{\text{CMB}} + y_\alpha T_k + y_c T_k}{1 + y_\alpha + y_c} \quad (2)$$

It can be interpreted as the weighted average of the CMB temperature and T_k . T_k is the kinetic temperature of the IGM. Here y_c and y_α are the contributions to the spin temperature from collisions and Ly- α photons respectively. If Ly- α pumping or collisions are efficient, their weight factors will increase and the spin temperature will couple to the kinetic temperature. These processes will be explained in their respective sections.

2.3. The Wouthuysen-Field effect

The Wouthuysen-Field effect is sometimes named Ly- α pumping. It is capable of “transporting” electrons to the excited hyperfine energy level.

For 21-cm radiation to be emitted, a photon needs to decay from the $1_1S_{1/2}$ state to the $1_0S_{1/2}$ state. Because we still see 21-cm radiation emitted nowadays (and even though the spontaneous decay rate A_{10} gives a long lifetime to the $1_1S_{1/2}$ state) there must be some mechanism that puts electrons in the $1_1S_{1/2}$ state.

Looking at figure (1) we see the possible transitions in the hydrogen atom. The dashed lines are not important for the level mixing process. This is because they have no influence on the electron level populations for the relevant levels. For an electron at rest in the ground state, that is, $1_0S_{1/2}$, there are two possible transitions, to $2_1P_{1/2}$ or to $2_1P_{3/2}$. These transitions correspond to different photon energies (and thus frequencies). Once in that level, the electron can then drop to the $1_1S_{1/2}$ level. This process of electrons moving from $1_0S_{1/2}$ to $1_1S_{1/2}$ (and vice versa) is called level mixing. A Ly- α photon (or one with a higher energy) is required to enable the initial excitation.

In the IGM where low particle densities dominate the Wouthuysen-Field effect is the most efficient in decoupling the spin temperature from T_{CMB} (Chen and Miralda-Escudé, 2004). Ly- α photons exist naturally in the Universe from conventional astrophysical sources that emit radiation in the UV spectrum, i.e. stars, nebulae, etc. However, we need to consider the possibility that dark matter decay or annihilation has a contribution to the 21-cm background radiation field. How much influence this will have depends mostly on the type of dark matter particle considered. The "decay channel" determines what sort of particles (and how many) will be created after decay. Annihilations can create two or more photons and provide another source of photon injection. However, because there is no way for us to know the accurate energy spectrum of dark matter we have to make some assumptions there. Those will be treated in more detail later.

A Ly- α photon is scattered many times ($\sim 10^5$) in the IGM before it shifts out of the Ly- α resonance where it is no longer able to excite electrons in the singlet state (Furlanetto et al., 2006). This repeated scattering with the IGM causes the spin temperature to couple to the kinetic temperature.

Relating this physics to the equations, we need to model its influence. Field (1958) has written the weight factor y_α as

$$y_\alpha = \frac{T_* P_{10}}{T_k A_{10}} \quad (3)$$

where P_{10} is the de-excitation rate coefficient for the hyperfine levels in units of sec^{-1} for Ly- α photons. The precise definition of P_{10} is

$$P_{10} = \frac{4}{27} P_\alpha \quad (4)$$

where P_α is the Ly- α scattering rate.

$$P_\alpha = \frac{4\pi J_\alpha \sigma_\alpha}{h_p \nu_\alpha} \quad (5)$$

J_α is the flux originating from Ly- α photons, $\sigma_\alpha = \frac{\pi e^2 f_{12}}{m_e c}$ is the integrated Ly- α scattering cross section. h_p is the Planck constant and ν_α is the frequency of the Ly- α transition. e is the electron charge, m_e is the electron mass and f_{12} is the oscillator strength of the Ly- α transition with value 0.416. P_{10} , P_α and σ_α have been written by Ciardi and Madau (2003).

Combining this, the "full" form of the y_α weight becomes

$$y_\alpha = \frac{1}{h_p \nu_\alpha} \frac{16\pi^2 T_* e^2 f_{12}}{27 A_{10} m_e c} \frac{J_\alpha}{T_k} \quad (6)$$

Note that the 1,0 indices indicate a transition from the hyperfine quantum number F 1 to 0.

However, Chuzhoy and Shapiro (2006) have pointed out that eqn. (6) combined with eqn. (2) is not entirely correct because it does not properly take the photon energy change due to atomic recoil into account. When a Ly- α photon excites or ionizes an atom, momentum transfer occurs. This momentum is partially transferred to the kinetic energy of the atom. This is the energy change due to atomic recoil. However, one should also acknowledge that there is an extra energy loss for the photon due to the hyperfine splitting of the atom. Take for example the excitation of H I. When a photon excites it to a higher hyperfine energy level it is absorbed. The energy is partially distributed to exciting the electron in a higher state. Any eventual "excess" in energy goes into the kinetic energy of the atom. In time the excited state will decay to a lower lying hyperfine state. The energy of the resulting photon is then determined by which hyperfine level the electron decays to. Chuzhoy and Shapiro (2006) have recognized that this effect should be taken into account. Therefore, one should multiply eqn. (6) by

$$s_\alpha = e^{-0.37(1+z)^{1/2} T_k^{-2/3}} \left(1 + \frac{0.4}{T_k}\right)^{-1} \quad (7)$$

It is easily seen that this effect is more important for low-energy photons because the energy difference in the hyperfine level splitting has relatively more impact for them than high-energy photons.

2.4. Atomic collisions

Atomic collisions are heavily dependent on the number density of particles (which are $\propto (1+z)^3$) in the IGM, making them especially efficient at higher redshifts, but comparatively weaker at low redshifts. Several collision processes exist, but all involve the IGM. Free electrons, protons and even other hydrogen atoms are some of the particles that make up the IGM.

Recall that to modify the spin temperature the number densities of the hyperfine ground states have to be changed. Collisions do this by interchanging electrons with different spins. Just like Ly- α pumping, repeated collisions in the IGM drive the spin temperature towards the kinetic temperature.

Just like the Wouthuysen-Field effect, collisions have a weight factor associated with them as well to model the physics. The y_c weight has been defined as

$$y_c = \frac{T_*}{A_{10}T_k} \left[C_H(T_k) + C_E(T_k) + C_P(T_k) \right] \quad (8)$$

A_{10} is the spontaneous decay rate and has the value $2.85 \times 10^{-15} \text{ sec}^{-1}$. We use the Kuhlen et al. (2006) fitting formulae for the y_c collision factor:

$$C_H(T_k) \simeq n_H 3.1 \times 10^{-11} T_k^{0.357} e^{-32/T_k} \quad (9)$$

$$C_E(T_k) \simeq n_e \gamma_e(T_k) \quad (10)$$

$$C_P(T_k) \simeq 3.2 \frac{n_p}{n_H} C_H(T_k) \quad (11)$$

These are the collision contributions to the de-excitation rates for hydrogen atoms, free electrons and protons respectively. In these equations n_H , n_e and n_p are the hydrogen, electron and proton number densities. γ_e has been fitted by Liszt (2001) as

$$\log \gamma_e(T_k) = -9.607 + e^{-\frac{-\log(T_k)^{4.5}}{1800}} \log \sqrt{T_k} \quad (12)$$

It is the de-excitation rate factor for electrons originally calculated by Smith (1966). He also found that the rate coefficient for proton - hydrogen collisions is 3.2 times that of hydrogen - hydrogen collisions, which explains the 3.2 factor for the C_P expression. The C_H/n_H factor is partially derived from tabulated data by Zygelman (2005) (in the $1 \leq T_k \leq 300$ K regime) and Allison and Dalgarno (1969) multiplied by $\frac{4}{3}$ (in the $300 \leq T_k \leq 1000$ K regime).

2.5. Dark matter decay / annihilation

This section is devoted to the decay and/or annihilation products of DM. Both are processes that can inject particles into the IGM and able to modify the thermal and ionization history of the Universe. For DM to annihilate it needs to collide with another DM particle. The larger the cross section of the particle, the higher the collision probability because the effective area to collide on is larger. The decrease rate of the number of DM particles per baryon due to annihilations was given by Ripamonti et al. (2007) as

$$\dot{n}_{\text{DM}}(z) \simeq \frac{1}{2} n_{\text{DM},0}^2 \mathcal{N}_b(0) (1+z)^3 \langle \sigma v \rangle \quad (13)$$

where the factor $1/2$ is due to DM being composed of particles and anti-particles which introduces a factor $1/4$. This needs to be multiplied by 2 because each annihilation involves two particles. $\mathcal{N}_b(0)$ is the current baryon number density and it has the value $2.5 \times 10^{-7} \text{ cm}^{-3}$. $n_{\text{DM},0}$ is the present ratio of the DM number density over the baryon number density.

Since annihilations are proportional to $n_{\text{DM},0}^2$ we immediately see that they are much more efficient in high-density environments. For this reason some authors (see Chuzhoy (2008); Myers and Nusser (2008)) have recently considered the effects of DM annihilations in high-DM-density environments on the IGM. This effect will not be considered in our work.

The decay of a particle is a spontaneous process which depends mostly on the lifetime of a particle. It is not possible to tell when an individual particle will decay but averaged out over an entire distribution of source particles it is possible to derive an average decay rate. Through this Ripamonti et al. (2007) have defined the decrease rate of the number of DM particles per baryon due to decay as

$$\dot{n}_{\text{DM}}(z) = \frac{n_{\text{DM},0}}{\tau_{\text{DM}}} e^{-(t(0)-t(z))/\tau_{\text{DM}}} \simeq \frac{n_{\text{DM},0}}{\tau_{\text{DM}}} \quad (14)$$

where $t(z)$ is the time elapsed since the big bang to redshift z , ($t(z) \sim \frac{1}{H(z)}$). τ_{DM} is the mean lifetime of the particle. The last approximation in eqn. (14) holds if $\tau_{\text{DM}} \gg t(0)$, which is generally the case. Only because decay is a random process does this condition make sense from a physical viewpoint. A particle may have a lifetime longer than the age of the Universe but there will always be some particles that decay during the lifetime of the Universe itself. Only in cases where the lifetime is orders of magnitude larger than the age of the Universe does the decay rate get reasonably small that a particle can be called stable.

It makes a difference how a particle decays or annihilates for their influence on the IGM. Some products are more efficient at transporting their energy into the IGM. For example, electrons in a low-ionized Universe transfer a significant fraction of their energy into ionizations and excitations, creating cascade effects which influence the IGM thermal and ionization history more than an ultra-high energy photon which runs the risk of never even interacting with the IGM because the absorption probability is so much lower. Several decay channels are possible, including exotic particles but the DM products which we will consider are photons and electrons. To parametrize this channel we introduce variables $0 \leq \zeta_1 \leq 1$ (associated with photon products) and $0 \leq \zeta_2 \leq 1$ (associated with electron products) with the constraint that $\zeta_1 + \zeta_2 \leq 1$. If we set $\zeta_1 = 1$ then we assume that the only decay products are photons. We do this to conveniently allow for mixtures of decay products in our code.

If the decay products are photons, it makes sense to think about how this photon energy is distributed. The influence of photons on the IGM will increase as their energy gets lower because their mean free path gets much shorter. The mean free path of a photon is defined as

$$l = [n_b(z)\sigma(E)]^{-1} \quad (15)$$

It is the average path length a photon traverses between subsequent interactions. $\sigma(E)$ is a piecewise power law fitted by Zdziarski and Svensson (1989) defined as follows

$$\sigma(E) = \begin{cases} 0.75\sigma_{\text{H}}(E) & 13.6 \text{ eV} \leq E \leq 25 \text{ eV} \\ \sigma_{250}[E/(250\text{eV})]^{-2.65} & 25 \text{ eV} \leq E \leq 250 \text{ eV} \\ \sigma_{250}[E/(250\text{eV})]^{-3.3} & E \leq 250 \text{ eV} \end{cases} \quad (16)$$

$\sigma_{\text{H}}(E)$ is the photo-ionization cross section of hydrogen and σ_{250} is the cross section for 250 eV photons. The underlying assumption in obtaining these equations is that the IGM is mostly neutral, an assumption which holds for our redshifts of interest.

A high-energy photon will have a very small cross section so the scattering probability decreases. If we were to consider a one-photon DM product case (with an energy equal to the rest-mass energy of a DM particle) then the effects on the IGM would be minimal.

Partially because of this we choose to adopt a power-law approximation to the photon spectrum. We choose a power law with index $\alpha = 1$ to reflect that there will be comparatively more low-energy photons than high-energy photons as a rough approximation of a cascade of DM products.

$$\frac{dn}{dE} = \begin{cases} E^{-\alpha} & 0.01 \text{ eV} \leq E \leq \epsilon_{\text{DM}} \text{ eV} \\ 0 & \text{otherwise} \end{cases} \quad (17)$$

$\frac{dn}{dE}$ is the number of particles per energy bin. The limits have been chosen such that the low-energy part of the electromagnetic spectrum is covered and the upper limit for the theoretical maximally attainable energy of a photon: the rest-mass energy.

This is where the difference between our approach and other authors (Ripamonti et al., 2007) is the largest. Ripamonti et al. (2007) assume that the dark matter energy spectrum is essentially mono-energetic and define an average energy per dark matter particle per baryon. The evolution of the average energy and number density is then modeled through energy and number losses through the relevant mechanisms (Compton scattering for photons for example). Assuming mono-energeticity however only allows for a single type of DM product, which may not be a fair assumption. This is why we choose to model the energy spectrum with a power-law to model the influence of a cascade of DM products. Our motivation for doing this is because other astrophysical systems have comparable energy spectra.

We assume that for photons the photo-ionization and Compton scattering mechanisms inject energy into the IGM. Our energy spectrum is taken to be independent of redshift, essentially assuming that the energy spectrum from DM products does not change in time. For a WIMP DM candidate whose cascaded products transfer most of their energy into the IGM this is a fair assumption.

For every DM candidate, n_{DM} and τ_{DM} will be taken from the literature.

2.6. Fractional energy absorbed by the IGM

Since we consider electrons and photons as DM products we need to analyze how much of their energy is transferred to the IGM. The amount transferred is dependant on the type of particle. We distinguish photons and electrons and will treat them in that order.

Two energy transferring processes are important for photons: photoionization and Compton scattering. Photoionization is the process of a photon hitting an atom and ionizing it, creating a free electron. For simplicity, we will not add these electrons to the free electron fraction x_e . Instead, the absorption probability of this process will be used to derive an absorbed fraction for photons through photoionization. Compton scattering is the process of a photon scattering off an electron, thereby losing energy in the process. This energy is transferred to the electron, which can be excited to a higher state or the atom may even be ionized.

Photons are only able to transfer energy to the IGM if their energy is > 13.6 eV. For our analysis we need to derive a normalization constant C first:

$$C \int_{0.01}^{\epsilon_{DM}} \frac{dn}{dE} E dE = \zeta_1 \epsilon_{DM} \quad (18)$$

Note that the integral limits are given in eV. Because of this low lower limit C will have a value close to 1, but it is a correction nonetheless. ϵ_{DM} is the rest mass energy of the dark matter particle, $\frac{dn}{dE}$ is the energy spectrum. Recall that ζ_1 is the fraction of energy going into photons. The total energy absorbed into the IGM depends on the absorption probability. Generally, for a photon with an energy E traveling a distance dx the absorption probability is given by

$$P_{abs} = n_b \sigma_E(E) dx \quad (19)$$

dx here is the length of a cosmological line element, which is $c/H(z)$. To extend this absorbed fraction to an energy spectrum, the absorbed fraction of energy is given by

$$E_{abs} = n_b C \int_{13.6}^{\epsilon_{DM}} \frac{dn}{dE} E \sigma_E dE dx \quad (20)$$

The fractional energy absorbed due to Compton scattering is given by (see also Ripamonti et al. (2007))

$$E_{abs} = \frac{c}{H(z)} \sigma_T \xi g(\xi) n_e \quad (21)$$

where $\xi = E/(m_e c^2)$. σ_T is the Thomson cross section and n_e is the electron number density. Note that since Compton scattering is only effective at high energies it does not matter if an electron is free or bound. Therefore n_e includes free and bound electrons. $g(\xi)$ is defined by Zdziarski and Svensson (1989) equation (4.9) as

$$g(\xi) = \frac{3}{8} \left[\frac{(\xi - 3)(\xi + 1)}{\xi^4} \ln(1 + 2\xi) + \frac{2(3 + 17\xi + 31\xi^2 + 17\xi^3 - 10\xi^4/3)}{\xi^3(1 + 2\xi)^3} \right] \quad (22)$$

A convenient quantity to work with is the absorbed fraction f_{abs} . This is simply the ratio of eqn. (20) plus eqn. (21) over the total injected energy ϵ_{DM} . This represents the energy absorbed in the IGM over the total energy available.

The absorbed fractions for free electrons are well known. Through Monte-Carlo simulations Shull and van Steenberg (1985) have obtained expressions for f_{abs} for the electron case. We can use these for the case when we have electrons as DM products. Shull and van Steenberg (1985) distinguish several energy contributions, namely the fraction of energy that goes into heating, secondary ionizations and secondary excitations for H I and He I. Functional forms for these have been fitted. Form 1 to be used for heating is $\chi_H = C[1 - (1 - x^a)^b]$ and form 2 to be used for secondary ionizations and excitations is $\chi_I = C(1 - x^a)^b$. The C, a, b factors are different for all three processes. Heating has $C = 0.9971$, $a = 0.2663$ and $b = 1.3163$. Secondary ionizations have $C = 0.3908$, $a = 0.4092$ and $b = 1.7592$. Secondary excitations have $C = 0.4766$, $a = 0.2735$ and $b = 1.5221$. These values only apply for the case of neutral hydrogen. The factors for He I can be found in the Shull and van Steenberg (1985) paper.

It should be noted that these functional fits are only valid for energies greater than 100 eV. Since we treat energies in the range $13.6 \text{ eV} \leq E \leq 100 \text{ eV}$ as well we should realize that through using these formula we underestimate the low-energy electron contribution to heating and that we overestimate the low-energy electron contribution to ionizations.

2.7. Determining kinetic temperature evolution

To calculate the spin temperature the kinetic temperature of the IGM needs to be known. At these high redshifts, the gas in the IGM can heat up through Compton heating and cool down through adiabatic cooling. The ‘‘classical’’ equation that describes the temperature evolution with redshift is given by

$$(1+z)\frac{dT_k}{dz} = 2T_k - \frac{l_\gamma x_e}{H(z)(1+x_e)}(T_{\text{CMB}} - T_k) \quad (23)$$

with l_γ defined as

$$l_\gamma = \frac{8\sigma_T a_R T_{\text{CMB}}^4}{3m_e c} \quad (24)$$

In expression 24, m_e is the electron mass, σ_T is the Thomson scattering cross section, a_R is the radiation constant. l_γ has units of sec^{-1} and denotes the Compton cooling time. The second term of eqn. (23) has been obtained by calculating the radiation drag force from the isotropic CMB radiation field on a distribution of electrons.

x_e is the ionized fraction which we take from RECFAST. RECFAST (Seager et al., 1999) is a program that (numerically) calculates the ionization fraction as a function of z due to the influence of CMB photons, conventional sources are not included. By taking this data from RECFAST without any modifications we are assuming that DM products have no influence on the ionization fraction. In doing so we are using values that are lower than they should be. But this will not introduce significant bias because DM products can only increase the ionized fraction slightly. This estimate matters for absorbed fractions, Compton heating and number densities of free electrons and protons. We include figure (5) left hand panel for the ionized fraction.

The first term on the RHS in (23) is the adiabatic cooling term ($\propto (1+z)^2$) and the second term is the Compton heating term. In the Compton heating term it is the difference between T_k and T_{CMB} that causes them to couple, i.e. if $-(T_{\text{CMB}} - T_k)$ is larger than zero (i.e. T_k is larger than T_{CMB}), so will $T'_k(z)$ be less than zero (a downward slope); this is because $dt/dz < 0$. Therefore, the larger the difference between the two, the faster they will couple. For the redshift range $\sim 200 \leq z \leq 1100$ the kinetic temperature is coupled to the CMB temperature because of the residual free electrons left over from recombination which keep the gas thermalized with the CMB temperature. For $z \lesssim 200$ the IGM loses its coupling with these residual free electrons and will cool down adiabatically as $(1+z)^2$.

Since photons and electrons are able to supply energy that contributes to heating to the IGM, eqn. (23) needs to be extended with the following terms:

$$-\zeta_1 \frac{2}{3k} \frac{1}{H(z)(1+z)} \dot{n}_{\text{DM}} f_{\text{abs}} \chi_H \epsilon_{\text{DM}} \quad (25)$$

$$-\zeta_2 \frac{2}{3k} \frac{1}{H(z)(1+z)} \dot{n}_{\text{DM}} \chi_H \epsilon_{\text{DM}} \quad (26)$$

where f_{abs} in eqn. (25) is the absorbed fraction for photons derived earlier and χ_H in eqn. (25) and (26) is the fraction of energy of the absorbed electrons that goes into the IGM as heating (Shull and van Steenberg, 1985). Using a factor $2/3k$ means we are using an ideal-gas approximation.

2.8. The background radiation arising from DM decay/annihilations

Since WIMP DM particles decay or annihilate, their products can interact with the IGM. The extent of the interaction depends on the type of particle considered. Here we study the following WIMP particles: decaying sterile neutrinos, decaying light dark matter (LDM), annihilating LDM and exciting dark matter (XDM).

We have seen in the definition of the y_α coupling coefficient for the spin temperature that it is proportional to the flux of the resulting radiation. To determine the strength of Ly- α coupling we need to determine the flux. The angle-averaged radiation intensity due to decaying or annihilating dark matter is given by Madau et al. (1997) as

$$J_\alpha = \frac{n_{\text{H}}^2 h_p c}{4\pi H} \left[x_e x_p \alpha_{2^2P}^{\text{eff}} + x_e x_{\text{HI}} \gamma_{\text{eH}} + \dot{E} n_b / (n_{\text{H}}^2 h_p y_\alpha) \right] \quad (27)$$

The first term describes the effect of recombinations on the flux, the second term describes the ionizations due to the impacts of free electrons on neutral hydrogen and the last term describes the influence of the DM products on the flux. In this equation x_e , x_p and x_{HI} represent the free electrons, protons and neutral hydrogen number density with respect to the total hydrogen number density n_{H} . Originally the Madau et al. (1997) energy injection term (\dot{E}) was energy injection per hydrogen atom. Since we have energy injection per baryon, we have to multiply the last term with $\frac{n_b}{n_{\text{H}}}$. In eqn. (27) this has already been done. γ_{eH} has been defined by Osterbrock (1989) as

$$\gamma_{\text{eH}} \approx 2.2 \times 10^{-8} \text{ cm}^3 \text{ s}^{-1} \exp(-11.84/T_4) \quad (28)$$

where $T_4 = \frac{T_k}{10^4 \text{ K}}$. $\alpha_{2^2P}^{\text{eff}}$ is

$$\alpha_{2^2P}^{\text{eff}} = 1.67 \times 10^{-13} \left(\frac{T_k}{10^4} \right)^{-0.91 - (2/75) \log_2(T_k/10^4)} \quad (29)$$

This is a fit to the Pengelly (1964) recombination coefficient down to the 2^2P level. For completeness, the definition of $H(z)$ used in this document is

$$H(z) = H_0 \sqrt{\Omega_{\text{m}}(1+z)^3 + \Omega_{\Lambda}} \quad (30)$$

Here we take a flat Universe with $\Omega_{\text{m}} = 0.24$ and $\Omega_{\Lambda} = 0.76$. At our redshifts of interest ($\sim 10 < z < \sim 1100$) the Ω_{m} contribution is clearly the most important one for the evolution of $H(z)$. The Universe is matter dominated in this redshift range.

To have a significant effect on decoupling T_s from T_{CMB} the Wouthuysen-Field effect must be strong enough. This can be achieved by having a sufficiently intense radiation field. The radiation field around the Ly- α transition needs to fulfill the following condition:

$$J_\alpha > J_{\text{th}} = 9 \times 10^{-23} (1+z) \text{ erg cm}^{-2} \text{ s}^{-1} \text{ Hz}^{-1} \text{ sr}^{-1} \quad (31)$$

where the th subscript indicates the thermalization field needed (Ciardi and Madau, 2003). This is obtained through determining the minimum strength of the weight factor y_α required to couple the spin temperature to the kinetic temperature.

2.9. Relevant quantities

Several DM candidates will be considered. For convenience I will list the relevant quantities per candidate. Ripamonti et al. (2007) considered sterile neutrinos, LDM and neutralinos for their papers. The effects of neutralinos were found to be negligible, however, we will include them to see if their effects may be observable if their product energy is spread over a range of energies. The sterile neutrinos and LDM parameters were chosen for their maximal contribution to heating.

Candidate name	E(eV)	$\tau_{DM}(s)$	$\langle\sigma v\rangle(\text{cm}^3 \text{s}^{-1})$
Sterile neutrino	25×10^3	9.67×10^{25}	does not annihilate
Neutralino	100×10^9	irrelevant	2×10^{-26}
LDM	10×10^6	4×10^{25}	2.4×10^{-28}
Exciting DM	50×10^9	does not decay	0.254×10^{-26}
Minimal dark matter	$20 - 60 \times 10^9$	does not decay	4×10^{-24}

These values have been taken from the following papers: Ripamonti et al. (2007); Mapelli et al. (2006); Cholis et al. (2008a); Cirelli and Strumia (2008).

2.9.1. Sterile neutrinos

Sterile neutrinos have a very small cross section for interaction, making annihilations negligible. Therefore we will only consider their decay. The decay channel is the most important quantity. A sterile neutrino decays into an active neutrino and a photon. Since an active neutrino is thought not to interact with the IGM only half of the rest-mass energy of a sterile neutrino can be injected into the IGM. This is reflected in the absorbed fraction figures (Figure 2) as well. The lifetime τ_{DM} has been given by Mapelli and Ferrara (2005) as

$$\tau_{DM} = 9.67 \times 10^{25} \left(\frac{m_{\nu s} c^2}{25 \text{keV}} \right)^{-5} \left(\frac{1.55 \times 10^{-11}}{\sin^2 \theta} \right) \quad (32)$$

which holds for sterile neutrinos with rest mass energies > 24 keV. θ is the mixing angle which is a general neutrino property. For completeness, the lifetime for energies between 3.5 and 24 keV is given by

$$\tau_{DM} = 2.23 \times 10^{27} \left(\frac{m_{\nu s} c^2}{10 \text{keV}} \right)^{-5} \left(\frac{6.6 \times 10^{-11}}{\sin^2 \theta} \right) \quad (33)$$

2.9.2. Neutralinos

Neutralinos are massive particles (100 GeV in our case). Therefore if they decay their lifetimes must be very short and thus they cannot be DM candidates. Then, if neutralinos do exist they must be stable and decay is not important (Mapelli et al., 2006). Therefore we will treat neutralino annihilation only. Padmanabhan and Finkbeiner (2005) considered a thermally averaged redshift independent cross section, which we will adopt as well. It is given by

$$\langle\sigma v\rangle = 2 \times 10^{-26} \text{cm}^3 \text{s}^{-1} \quad (34)$$

2.9.3. Light Dark Matter

The LDM lifetime has been derived by Hooper and Wang (2004) as

$$\tau_{DM} = 4 \times 10^{26} \left(\frac{m_{LDM}}{\text{MeV}} \right)^{-1} \quad (35)$$

We will be considering 10 MeV LDM particles. The thermally-averaged cross section has been given by Ripamonti et al. (2007) as

$$\langle\sigma v\rangle \leq 2.2 \times 10^{-29} f_{\text{abs}}^{-1} \left(\frac{m_{LDM} c^2}{\text{MeV}} \right) \quad (36)$$

f_{abs} is a function of redshift which would make $\langle\sigma v\rangle$ redshift-dependent as well. However, for simplicity we will adopt the largest absorbed fraction over the redshift regime $10 \leq z \leq 1100$. Since LDM is thought to be able to purely decay or annihilate into a single product the theoretical maximally attainable absorbed fraction is ~ 1 .

2.9.4. Exciting Dark Matter

XDM is thought to annihilate to explain the e^-e^+ excess coming from the Galactic Halo. Cholis et al. (2008b) worked out a model to explain the positron excess measured in several experiments, like HEAT (High-Energy Antimatter Telescope) and to explain the future Payload for Antimatter Matter Exploration and Light-nuclei Astrophysics experiment (PAMELA) results for the positron fraction. We will use their derived parameters to see what effects their DM candidate might have. For simplicity we will use their HEAT data fit with a Navarro-Frenk-White (NFW) density profile, using a carrier particle with $m_\phi = 0.1$ GeV. This carrier particle determines the decay channel and in this case it is electron-positron pairs. For a 50 GeV particle which annihilates and creates e^-e^+ , the cross section is

$$\langle\sigma v\rangle = 0.058 \times 10^{-26} \text{ cm}^3 \text{ s}^{-1} \quad (37)$$

The choice for this cross section is made because the effects of this decay channel on the thermal history of the Universe will be largest due to having the lowest energy and largest cross section.

2.9.5. Minimal Dark Matter

In an attempt to explain the preliminary PAMELA results, Cirelli and Strumia (2008) have considered the existence of a type of DM particle called minimal dark matter (MDM). The PAMELA experiment predicts a positron excess coming from the Galactic halo and it is thought this excess might be DM products originating from annihilation or decay. The energy spectrum found by them is E^{-p} with $p = 2.64 \pm 0.06$. This spectrum is valid for the energy range 20 to 60 GeV. Using a boost factor of 100 we obtain a cross section of

$$\langle\sigma v\rangle = 4 \times 10^{-24} \text{ cm}^3 \text{ s}^{-1} \quad (38)$$

2.10. Constraining DM through the 21-cm background

What we actually observe on the sky (at 21 cm) is the 21-cm background. This background has an average temperature associated with it.

Using the radiative transfer equation in Rybicki and Lightman (1979) for a ray propagating through a cloud in the Rayleigh-Jeans limit ($h_p\nu \ll kT$) we have

$$T_b = T_{\text{CMB}}(0)e^{-\tau_\nu} + T_k(1 - e^{-\tau_\nu}) \quad (39)$$

where T_k is the cloud temperature and T_b is the brightness temperature which is defined as the temperature of a blackbody emitter with the same brightness (I_ν) at that frequency. For low optical depths (as is the case in the IGM) the brightness temperature is distinct from the gas temperature, but roughly equal to T_{CMB} . Note that a cloud is not really a cloud per se but rather any part of the IGM. The flux observed at earth can then be expressed as

$$\delta T_b = \frac{T_s - T_{\text{CMB}}}{1+z} (1 - e^{-\tau_\nu}) \quad (40)$$

which for $\tau_\nu \ll 1$ can be approximated as

$$\delta T_b = \frac{T_s - T_{\text{CMB}}}{1+z} \tau_\nu \quad (41)$$

We can interpret δT_b as a deviation of T_s from a blackbody spectrum. The optical depth of the neutral IGM at $21(1+z)$ cm is given by the following expression:

$$\tau_\nu = \frac{3c^3 h_p A_{10} x_{\text{HI}}}{32\pi k \nu_\alpha^2 T_s H(z)} \quad (42)$$

x_{HI} is the neutral hydrogen fraction. We now have all the ingredients required to compute the effects that DM has on the IGM.

As an approximation to other authors' results we create a mono-energetic spectrum by taking a normalized gaussian peaked at the rest mass energy of the DM particle. This gaussian is designed to be very small as to be as sharply peaked as possible.

$$\frac{dn}{dE} = \frac{1}{\sqrt{2\pi\sigma^2}} \exp\left(-\frac{(E - \epsilon_{\text{DM}})^2}{2\sigma^2}\right) \quad (43)$$

3. Results

In this section the most notable results will be displayed. A short explanation of the specifics of each figure will be given. All lines displayed in the respective graphs are subject to the same physical laws, therefore section 4 will go into detail about the general physics that modifies the thermal history of the universe and other relevant physics. The influence of DM on the thermal history will be described in this section.

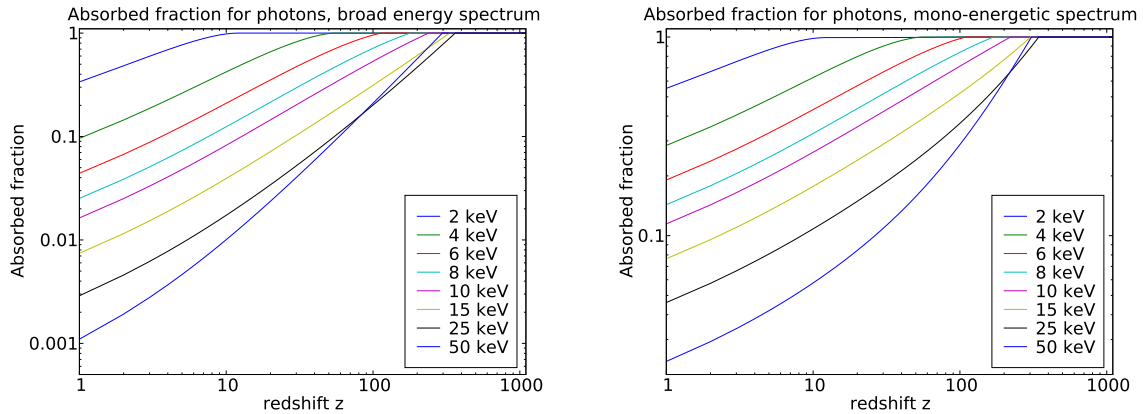


Fig. 2: Comparison of the influence of spectra on the absorbed fractions for photons as decay products. Left panel: shows the absorbed fraction for photons for several energies with powerlaw index 1. Right panel: Absorbed fraction for photons for several energies with mono-energetic energy spectrum.

Shown in Figure (2) is the absorbed fraction for photons as a function of redshift. The energies considered are particularly relevant for sterile neutrinos since they have rest-mass energies on the order of 2 to 50 keV. The difference between the two panels is the shape of the energy spectrum of the DM products. The left hand panel has an energy spectrum defined as $dn/dE = E^{-1}$ whereas the right hand panel has a mono-energetic spectrum (see eqn. (43) for the exact spectrum definition).

The range of energies displayed in the figures is from 2 to 50 keV. For the heaviest sterile neutrino candidate with an energy of 50 keV, the absorbed fraction for an energy spectrum at a redshift of 1 is about 150 times larger than for a mono-energetic spectrum. For the lightest sterile neutrino candidate with an energy of 2 keV, the absorbed fraction for an energy spectrum at redshift 1 is about 8 times larger than for a mono-energetic spectrum.

The influence of Compton scattering is such that for very high energies there always is a small fraction of energy absorbed into the IGM, whereas the absorbed fraction for photo-ionization (in the limit of very high energies) goes to a negligible amount. This has the result that even high energy photons should not be discounted for energy transfer into the IGM.

Note that the absorbed fraction for Compton scattering is proportional to the number density of electrons which increases as $(1+z)^3$, making the contribution to the absorbed fraction from Compton scattering non-negligible at high redshifts, even for lower-energy photons.

This is partly the cause of the apparent oddity at photon energies of 25 and 50 keV whose lines cross at redshift $\sim 100-200$ (depending on the panel). For both the mono-energetic and broad energy spectrum case the energy absorbed fraction of 50 keV exceeds that of 25 keV at high redshifts. This clearly cannot be due to photoionization because this process gets less efficient at higher photon energies. We conclude that this must be from Compton scattering which gets more and more effective until the 511 keV energy is reached, at which point the energy absorbed fraction due to Compton scattering starts to decrease again. The 50 keV photon energy absorbed fraction for the mono-energetic case starts to take over the energy absorbed fraction for the 25 keV photon much faster than for the broad energy spectrum case because Compton scattering is more influential in these high energy regimes. This explains the difference in shapes of the blue and black lines (corresponding to 50 and 25 keV respectively) in both panels of Figure (2).

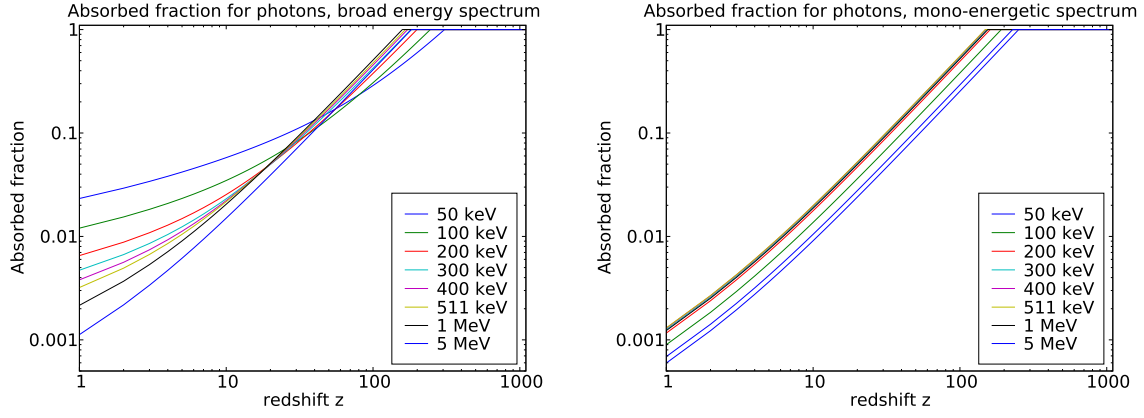


Fig. 3: Comparison of the influence of spectra on the absorbed fractions for photons. Left panel: shows the absorbed fraction of photons for several energies with powerlaw index 1. Right panel: shows the absorbed fraction of photons for several energies with mono-energetic energy spectrum.

The next set of absorbed fractions (see Figure 3) displays the higher photon energy cases to illustrate the influence of Compton scattering on the absorbed fraction. Taking a look at the right hand panel of Figure (3) we see that the highest absorbed fraction is obtained by the 511 keV photon because Compton scattering is the most efficient at that energy. When examining the lines from low to high energies it is seen that the absorbed fraction starts out low, then slowly increases to a locus at 511 keV at which point the absorbed fraction starts to decrease again. This is the reason why the lowest and highest energies (50 keV and 5 MeV) are close to each other. For the broad energy spectrum case (corresponding to the left hand panel of the same figure) there is considerably more difference between the absorbed fractions for the photon energies. The low-redshift behaviour is due to the influence of photo-ionization. For a spectrum with a cutoff at low energies there will be enough photons with energies low enough such that photo-ionization is able to drive the overall absorbed fraction up. As the spectrum gets broader over a wider energy range the photo-ionization influence decreases and the overall absorbed fraction drops.

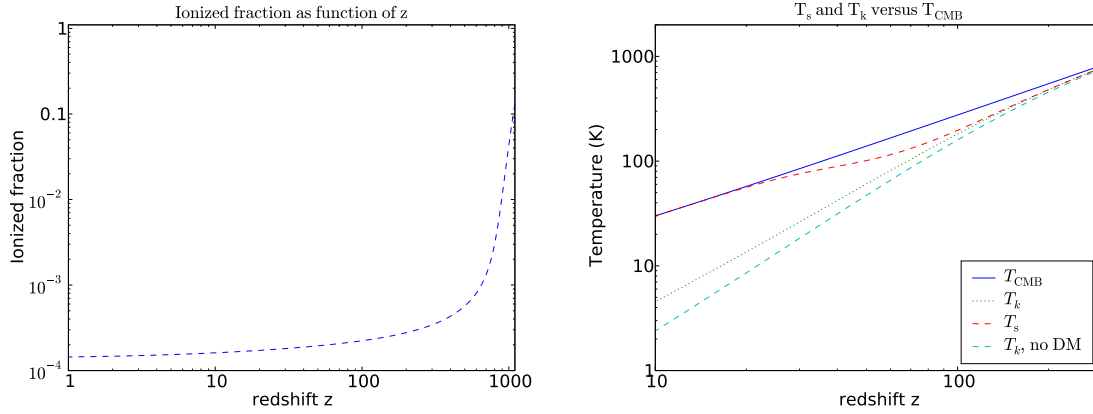


Fig. 4: Left panel: shows the ionized fraction due to CMB photons only obtained from RECAST. Right panel: T_s (red dashed line) and T_k with (without) DM influence, green dotted line (light-blue dashed line), T_{CMB} (solid blue line) as function of redshift z for 10 MeV annihilating LDM into electrons with RMF absorbed fraction fit.

The left hand panel of Figure (4) gives the ionized fraction as a function of redshift, obtained through running RECAST as explained earlier in this report. We will be using the data in the redshift range 10 to 1100. We see that our assumption for a neutral universe holds for redshifts 10 to ~ 600 . The reason the ionized fraction goes to 1 as z goes to 1100 is that before recombination every particle was ionized. Only after recombination does the ionized fraction go down through recombination in the redshifts afterwards. This ionization fraction history is due to the effects of CMB photons only. The expected reionization of the universe through stars and other conventional astrophysical sources therefore cannot be seen in this figure.

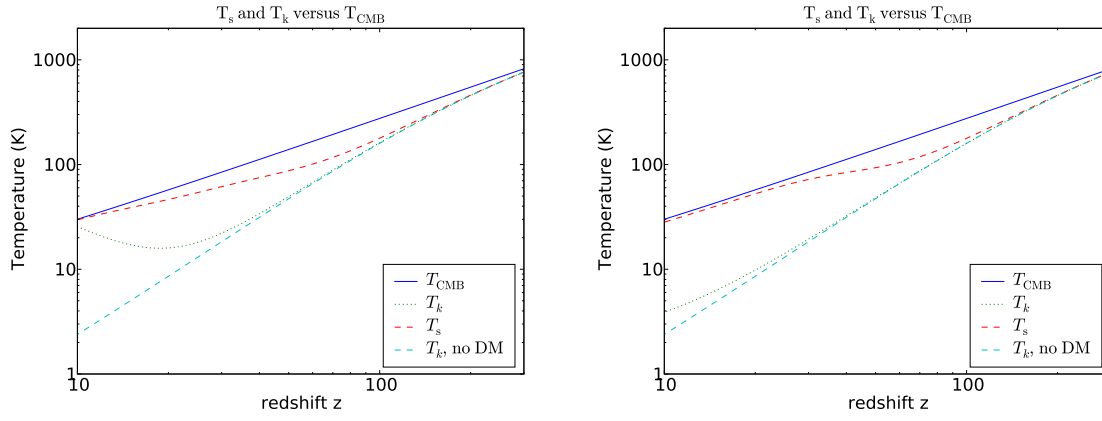


Fig. 5: Left panel: T_s (red dashed line) and T_k with (without) DM influence, green dotted line (light-blue dashed line), T_{CMB} (solid blue line) as function of redshift z for 10 MeV decaying LDM into electrons with RMF absorbed fraction fit. Right panel: T_s (red dashed line) and T_k with (without) DM influence, green dotted line (light-blue dashed line), T_{CMB} (solid blue line) as function of redshift z for 25 keV decaying sterile neutrinos into photons with RMF absorbed fraction fit.

The right hand panel of Figure (4) and both panels of Figure (5) display the results of our code with the Ripamonti et al. (2007) parameters and fit of the absorbed fraction. We see that all figures are in good agreement. For a discussion of these results, we refer to their paper.

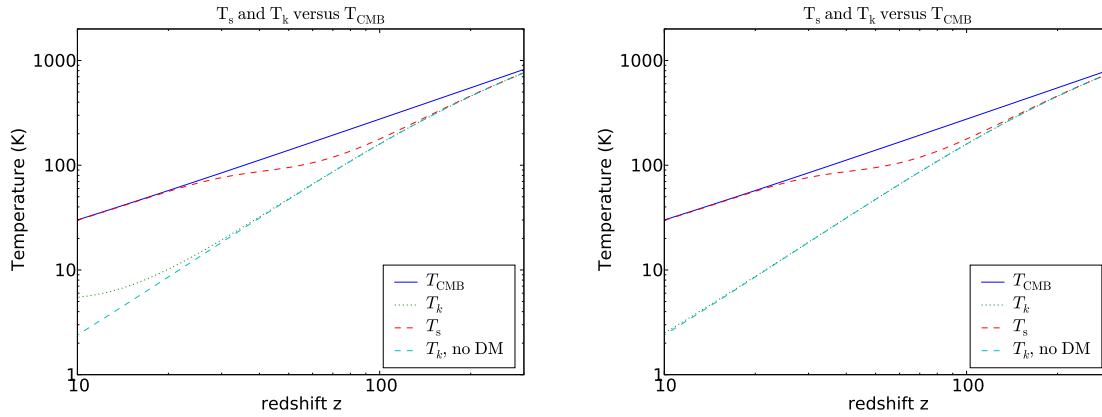


Fig. 6: Comparison of the thermal histories for 25 keV decaying sterile neutrinos. Left panel: T_s (red dashed line) and T_k with (without) DM influence, green dotted line (light-blue dashed line), T_{CMB} (solid blue line) as function of redshift z for 25 keV decaying sterile neutrinos into 10% photons with an energy spectrum $dn/dE = E^{-1}$. Right panel: T_s (red dashed line) and T_k with (without) DM influence, green dotted line (light-blue dashed line), T_{CMB} (solid blue line) as function of redshift z for 25 keV decaying sterile neutrinos into 10% photons with a mono-energetic energy spectrum.

One model of the thermal history with DM influence is given in Figure (6). The DM candidate considered are decaying sterile neutrinos transferring 10% of their energy into photons. We can immediately see that the shape of the energy spectrum has a profound influence on the evolution of the kinetic temperature. In this case, it makes the difference between a thermal evolution history differing from the standard case (without DM influence) or not. At redshift 10, the difference between the kinetic temperatures for the energy spectrum and mono-energetic energy spectrum case is roughly 3.5 Kelvin. We expect this because the absorbed fraction of photon energy is much higher for the spectrum case because of the higher photo-ionization cross section, causing more energy to be transferred into the IGM of which a part goes into heating. A single photon with an energy of 25 keV is more likely to traverse the Universe undisturbed, translating into a lower absorbed energy fraction. We should note however that the influence of this different kinetic temperature only has a marginal influence on the spin temperature. Because of this we should not expect it to be able to constrain the type of decay channel (energy spectrum versus mono-energetic energy spectrum) through the differential brightness temperature.

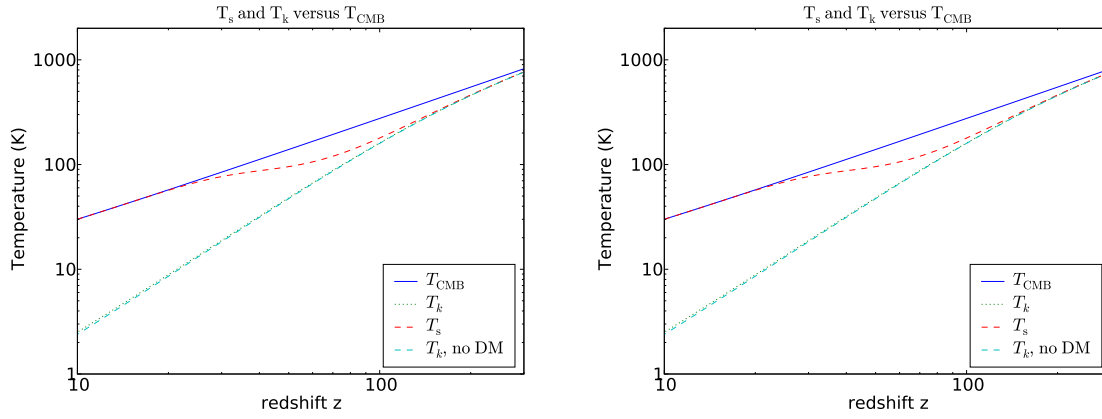


Fig. 8: Comparison of the thermal histories for 10 MeV annihilating LDM. Left panel: T_s (red dashed line) and T_k with (without) DM influence, green dotted line (light-blue dashed line), T_{CMB} (solid blue line) as function of redshift z for 10 MeV annihilating LDM into 5% photons & 5% electrons with an energy spectrum $dn/dE = E^{-1}$. Right panel: T_s (red dashed line) and T_k with (without) DM influence, green dotted line (light-blue dashed line), T_{CMB} (solid blue line) as function of redshift z for 10 MeV annihilating LDM into 5% photons & 5% electrons with a mono-energetic spectrum.

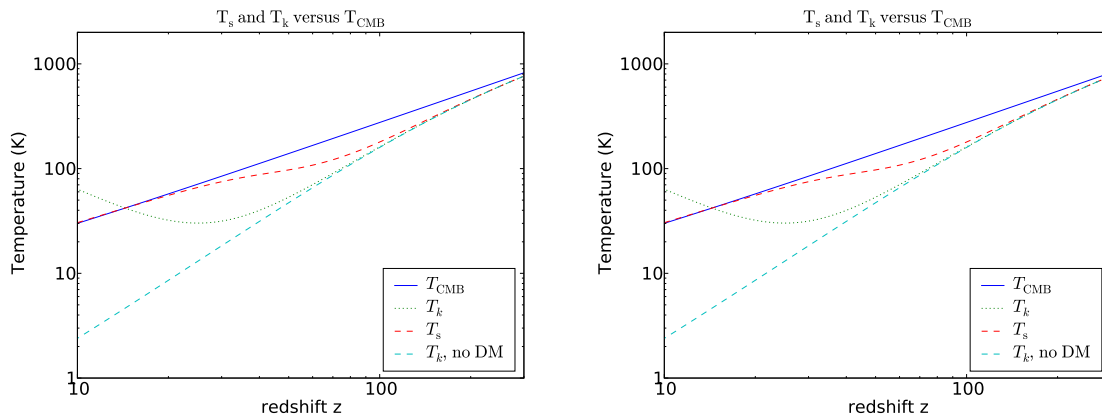


Fig. 7: Comparison of the thermal histories for 10 MeV decaying LDM. Left panel: T_s (red dashed line) and T_k with (without) DM influence, green dotted line (light-blue dashed line), T_{CMB} (solid blue line) as function of redshift z for 10 MeV decaying LDM into 10% electrons with an energy spectrum $dn/dE = E^{-1}$. Right panel: T_s (red dashed line) and T_k with (without) DM influence, green dotted line (light-blue dashed line), T_{CMB} (solid blue line) as function of redshift z for 10 MeV decaying LDM into 10% electrons with a mono-energetic spectrum.

Figure (7) is perhaps a trivial example, but it has a point that should be made nonetheless. For DM products decaying into purely electrons the evolution of the kinetic temperature will be identical because in our model we allow for immediate electron energy absorption into the IGM. The implementation of an energy spectrum for electrons would make no difference as Shull and van Steenberg (1985) derived an absorption fraction independent of the primary electrons' energy. It is found that this is a reasonable assumption to make. Another important thing to note is that electrons are able to efficiently transfer their energy into the IGM. This will be mostly apparent in the low-redshift kinetic temperature evolution: they are able to heat the gas to significant temperatures. The cause of derived high kinetic temperatures might be from electrons as DM products.

Figure (8) shows the effect of an 10 MeV annihilating DM particle. As a general rule, the mass of the DM candidate cannot be too large or else the annihilation rate (which is proportional to n_{DM}^2) will be too low to transfer enough energy into the IGM. Even though the mass of this annihilating LDM particle is equal to the mass of the decaying LDM particle the effect on the kinetic temperature is much smaller. This is because the decay rate is constant with redshift whereas the annihilation rate is proportional to $(1+z)^3$, making it more efficient at high redshifts. Therefore the influence of annihilations on heating the IGM is negligible. In comparison with the Ripamonti et al. (2007) results we find considerable difference in the thermal history because of our assumption that not all of the DM products consist of one particle type that are able to transfer energy into the IGM.

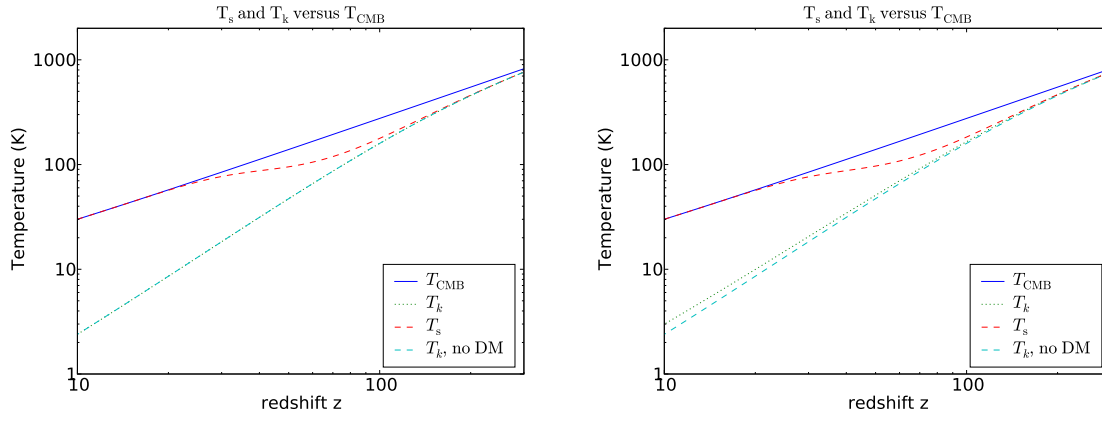


Fig. 9: Comparison of the thermal histories for 100 GeV annihilating neutralinos and 60 GeV annihilating MDM. Left panel: T_s (red dashed line) and T_k with (without) DM influence, green dotted line (light-blue dashed line), T_{CMB} (solid blue line) as function of redshift z for 100 GeV annihilating neutralinos into electrons with an energy spectrum $dn/dE = E^{-2}$, using the Myers and Nusser (2008) data, 10% of energy into electrons. Right panel: T_s (red dashed line) and T_k with (without) DM influence, green dotted line (light-blue dashed line), T_{CMB} (solid blue line) as function of redshift z for 60 GeV annihilating MDM into 10% electrons with an energy spectrum $dn/dE = E^{-2.64}$, using the Cirelli and Strumia (2008) data.

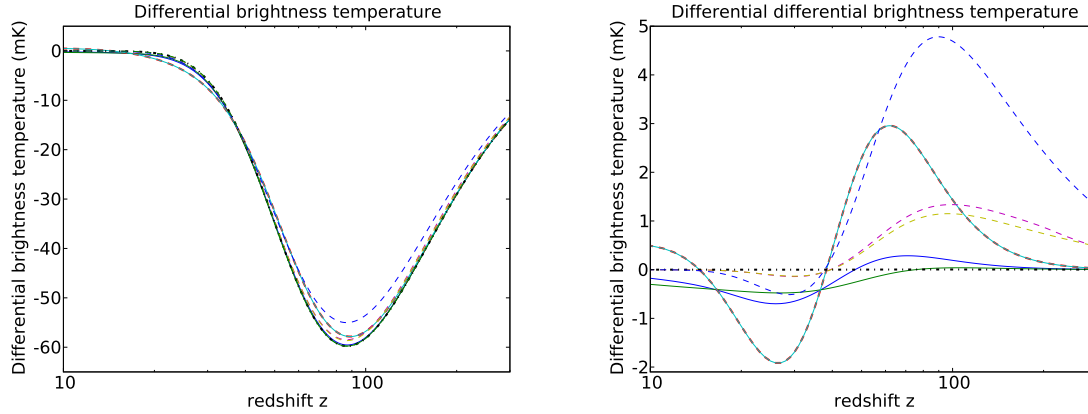


Fig. 10: Left panel: shows the differential brightness temperatures. Right panel: shows the differential differential brightness temperatures (with respect to the non-DM thermal history). For both panels, the dashed green line corresponds to the standard case without DM influence, solid blue line (solid green line) corresponds to 25 keV decaying sterile neutrinos with (without) an energy spectrum. Dashed red line (solid light-blue line) corresponds to 10 MeV decaying LDM with (without) an energy spectrum. Dashed purple (dashed yellow) line corresponds to 10 MeV annihilating LDM. Dash-dotted black line corresponds to 100 GeV annihilating neutralinos with an energy spectrum, dashed blue line corresponds to 60 GeV annihilating MDM with an energy spectrum.

Neutralinos and MDM are the two other DM candidates, displayed in Figure (9). For neutralinos, Myers and Nusser (2008) have determined that the spectrum of the electron energies has a slope of -2 . Also derived is that maximally 10% of the initial DM particle energy goes into electrons. In the left hand panel of Figure (9) we see that the kinetic temperature is not able to decouple from the “classic” kinetic temperature, which is a result of the low number density of neutralinos so that the effects of annihilations are negligible at low redshifts.

For MDM the results are interesting as well. Using an electron boost factor of 100 we obtain the right hand panel of Figure (9). The annihilation rate for an MDM particle will be low since MDM is a heavy particle just like the neutralino. It is more efficient in heating the IGM than the neutralino is, because the number density for a 60 GeV particle is just large enough to contribute, whereas for a 100 GeV particle it is too low. Slight heating of the IGM can be seen but it has no appreciable effect on decoupling the spin temperature.

It is interesting to note that heating is visible for the 60 GeV case but no longer so for the 100 GeV case (with both cases having 10% electrons as DM products). For the preliminary PAMELA results which extends to energies of 60 GeV (but with an expected much higher cutoff of 10^4 GeV) we expect that this source will produce no significant heating on the IGM.

In Figure (10) the differential brightness temperature is plotted. Most DM products modify this quantity from the standard case (which is of a Universe without DM influence on the thermal history). Even though it is possible for the signal to be visible in absorption (in theory) it is found that the effects of DM products are too small to do this. Instead, most DM products only produce a small deviation from the standard case without DM influence.

The standard case (dashed green line) shows the largest maximal amplitude in the differential brightness temperature. Generally we can conclude that DM products have the effect of decreasing this amplitude. This is to be expected since the coupling mechanisms tend to drive the spin temperature to the kinetic temperature. The kinetic temperature for the DM influenced universes tends to be higher than that of the classical case (which lacks heating effects by DM products). Because of this, the difference between the spin temperature and the CMB temperature generally will be smaller, decreasing the amplitude.

The light-blue line and the dashed red line are 10 MeV decaying LDM with electrons as their decay products. 10 MeV makes for a light particle and combined with the cosmological constraints on the amount of DM there is, their number density is very high. Since they have a reasonable average lifetime the decrease rate of the number of DM particles is high. Together with purely electrons as decay products this makes for one of the most efficient DM candidates in terms of their energy transfer into the IGM. However, even though all these circumstances are favorable for creating an easily-observable signal it turns out that this is not the case. They are superposed because the energy absorbed fraction is not a function of energy for this case.

Another DM candidate is 10 MeV annihilating LDM with a mixed spectrum (dashed purple and yellow lines). Mixed in this sense means that the decay products consist of 5% photons and 5% electrons. The lines are mostly superposed except for the redshift range where their decoupling effects are the strongest. Distinguishing the mono-energetic spectrum from the broad energy spectrum will be impossible in the near future, let alone distinguishing from the standard case.

25 keV decaying sterile neutrinos (the solid blue and green lines) have low mass making Ly- α pumping efficient. Therefore they are expected to efficiently decouple from the standard case at low redshifts because that is the redshift range where Ly- α pumping is efficient. However, it is seen that at low redshifts the lines are essentially superposed onto the standard case line.

60 GeV annihilating Minimal Dark Matter with electrons as decay products (the dashed blue line) will be hard to constrain at low redshift. Because it has virtually no contribution to Ly- α pumping because of its high restmass-energy it is superposed with the standard case up until a redshift of ~ 40 . For higher redshifts electron collisions start to play a role and the maximum difference in amplitude with respect to the standard case is quite significant. Constraining this particle is best done at redshift ~ 90 , but with sensitive equipment it could be done as early as redshift ~ 70 . It is the particle with the largest deviation from the standard case.

100 GeV annihilating neutralinos with electron decay products (the dash dotted black line) is superposed on the standard case. The number density for this particle is so low that the decrease rate of DM particles is too little to make Ly- α pumping or collisions important. For this reason this particle will not have a significant effect on changing the thermal history of the Universe.

The differential differential brightness temperature is perhaps a more intuitive quantity (see Figure (10)). It displays the deviation of the differential brightness temperature with respect to the standard case. The lines in the right panel correspond to the ones in the left panel. The “zero line” is the standard case. Easily seen is that the required resolution to distinguish the spectra of the DM candidate products from each other needs to be at least 0.5 mK, based on their signals. The value of the right-hand panel is that it immediately shows what candidates are easiest to constrain at low redshifts. As a rule the lightest particles will show the strongest decoupling because of the efficiency of Ly- α pumping on these. All remaining heavier particles are superposed with the standard case at low redshifts. The intermediate and higher-mass particles start to decouple at higher redshift ranges where collisions become more efficient.

4. Summary & discussion

All figures for all considered DM candidates can be found in the appendix. Only the most interesting ones are displayed in section (3). The specifics of the figures have been discussed in detail in the preceding section. This section will go into the details of the generic thermal evolution effects induced by other (non-DM) components of the Universe. All temperatures displayed are subject to the same physics with only the strength of the decoupling differing because of the different DM particle properties. Therefore we will discuss the general physics for all the thermal evolution history figures.

At high redshifts $z \gtrsim 300$ we see that the gas temperature is coupled to the CMB temperature. Thomson scattering of CMB photons on the residual electrons from recombination couples these temperatures. Around $z \sim 300$ the CMB photon field energy density becomes too low to couple the gas temperature and we see that it starts down to cool adiabatically (proportional to $(1+z)^2$). This can be clearly seen in the dashed light-blue line displayed in the thermal evolution history figures, which is the gas temperature without any DM product particle influence.

In some cases, DM product particles can have an influence on heating the IGM. The gas temperature with DM product particle influence is given by the dotted green line. If the decay products are electrons then we see considerable heating effects on the IGM. This is because electrons are able to efficiently transfer their energy into the IGM. For a low ionization fraction, 14 % of the electron energy goes to heating. The remainder of the energy is put into the excitation (36%) and the ionization (41%) of the IGM. This does not add up to 100% because the remainder of these percentages go into He I ionizations and excitations, which we do not consider (see also Shull and van Steenberg (1985)).

The spin temperature is given by the dash dotted red line. For most DM candidates and their influence the IGM is mostly visible in absorption in the differential brightness temperature because the spin temperature is lower than the CMB temperature. However, in some cases the combination of (1) heating of the IGM is strong enough that the gas temperature becomes very high at low redshifts and (2) Ly- α pumping through collisional excitations is efficient enough to enable the spin temperature to rise above the CMB temperature.

Since the next generation of radio telescopes is able to look out to redshifts of about ~ 11 the low-redshift behaviour of the differential brightness temperature is important. The differential differential brightness temperature (with respect to the spin temperature of an Universe without DM influence) is a more intuitive quantity. In Figure (10) left hand panel we see that to distinguish different particles from each other a resolution of at least 0.5 mK is required.

Constraining DM candidates through observations is possible in theory through observing the differential brightness temperature. In the ideal case every DM candidate has a unique spin temperature evolution which turns out not to be the case. In most cases a radically different spin temperature evolution is not attainable.

To distinguish DM candidates from each other with so many free parameters (the decay channel, the rest-mass energies, the cross sections and many others) proves to be difficult. The differential differential brightness temperature (see figure 10) left hand panel has an maximal amplitude of $\sim 1.5-5$ mK for different particles.

The influence that particles exert depends mostly on their number density. Combined with the cosmological constraints on the amount of DM there is in existence this fixes the number density of a given type of DM particle (with a given energy). This number density in turn modifies the annihilation rate or decay rate.

The products of DM candidates are essential for determining how energy is transferred into the IGM. Electrons have a short mean free path length and efficiently transfer energy into the IGM. For photons the photo-ionization and Compton scattering processes are relevant. The shape of the photon spectrum plays an important role in the absorption efficiency as well. Generally low energies transfer energy into the IGM efficiently through photo-ionization. Compton scattering is efficient around 511 keV and drops off slowly to both sides.

For coupling the spin temperature to the kinetic temperature Ly- α coupling and collisional coupling are important. The first one is dependent on the flux and favors high annihilation/decay rates combined with low restmasses. The latter is important at high redshifts (~ 50 - 200) because of the high number densities of particles.

It is found that even though some DM candidates have favorable parameters for attaining a radically different thermal history of the Universe it is not possible for them to actually do so, even while being given optimistic properties (like large cross-sections, photon spectra tending towards many low-energy photons, etcetera). The difference in differential brightness temperatures between particles of one type but slightly different parameters will be on the order of ~ 0.1 mK. Distinguishing them from one another will be impossible in the near future.

Bibliography

- K. Abazajian, G. M. Fuller, and W. H. Tucker. Direct Detection of Warm Dark Matter in the X-Ray. *ApJ*, 562:593–604, December 2001. .
- A. C. Allison and A. Dalgarno. Spin Change in Collisions of Hydrogen Atoms. *ApJ*, 158:423–+, October 1969. .
- Y. Ascasibar, P. Jean, C. Boehm, and J. Knödlseeder. Constraints on dark matter and the shape of the Milky Way dark halo from the 511-keV line. *MNRAS*, 368:1695–1705, June 2006. .
- G. Bertone, D. Hooper, and J. Silk. Particle dark matter: evidence, candidates and constraints. *Phys. Rep.*, 405:279–390, January 2005. .
- C. Boehm, D. Hooper, J. Silk, M. Casse, and J. Paul. MeV Dark Matter: Has It Been Detected? *Physical Review Letters*, 92(10):101301–+, March 2004. .
- A. Boyarsky, A. Neronov, O. Ruchayskiy, and M. Shaposhnikov. Constraints on sterile neutrinos as dark matter candidates from the diffuse X-ray background. *MNRAS*, 370:213–218, July 2006. .
- X. Chen and J. Miralda-Escudé. The Spin-Kinetic Temperature Coupling and the Heating Rate due to Ly α Scattering before Reionization: Predictions for 21 Centimeter Emission and Absorption. *ApJ*, 602:1–11, February 2004. .
- I. Cholis, L. Goodenough, and N. Weiner. High Energy Positrons and the WMAP Haze from Exciting Dark Matter. *ArXiv e-prints*, 802, February 2008a. .
- I. Cholis, L. Goodenough, and N. Weiner. High Energy Positrons and the WMAP Haze from Exciting Dark Matter. *ArXiv e-prints*, 802, February 2008b. .
- L. Chuzhoy. Impact of Dark Matter Annihilation on the High-Redshift Intergalactic Medium. *ApJ*, 679:L65–L68, June 2008. .
- L. Chuzhoy and P. R. Shapiro. Ultraviolet Pumping of Hyperfine Transitions in the Light Elements, with Application to 21 cm Hydrogen and 92 cm Deuterium Lines from the Early Universe. *ApJ*, 651:1–7, November 2006. .
- B. Ciardi and P. Madau. Probing beyond the Epoch of Hydrogen Reionization with 21 Centimeter Radiation. *ApJ*, 596:1–8, October 2003. .
- M. Cirelli and A. Strumia. Minimal Dark Matter predictions and the PAMELA positron excess. *ArXiv e-prints*, 808, August 2008. .
- A. D. Dolgov and S. H. Hansen. Massive sterile neutrinos as warm dark matter. *Astroparticle Physics*, 16:339–344, January 2002. .
- X. Fan, M. A. Strauss, D. P. Schneider, R. H. Becker, R. L. White, Z. Haiman, M. Gregg, L. Pentericci, E. K. Grebel, V. K. Narayanan, Y.-S. Loh, G. T. Richards, J. E. Gunn, R. H. Lupton, G. R. Knapp, Ž. Ivezić, W. N. Brandt, M. Collinge, L. Hao, D. Harbeck, F. Prada, J. Schaye, I. Strateva, N. Zakamska, S. Anderson, J. Brinkmann, N. A. Bahcall, D. Q. Lamb, S. Okamura, A. Szalay, and D. G. York. A Survey of $z_{\text{c}}5.7$ Quasars in the Sloan Digital Sky Survey. II. Discovery of Three Additional Quasars at $z_{\text{c}}6$. *AJ*, 125:1649–1659, April 2003. .
- X. Fan, M. A. Strauss, G. T. Richards, J. F. Hennawi, R. H. Becker, R. L. White, A. M. Diamond-Stanic, J. L. Donley, L. Jiang, J. S. Kim, M. Vestergaard, J. E. Young, J. E. Gunn, R. H. Lupton, G. R. Knapp, D. P. Schneider, W. N. Brandt, N. A. Bahcall, J. C. Barentine, J. Brinkmann, H. J. Brewington, M. Fukugita, M. Harvanek, S. J. Kleinman, J. Krzesinski, D. Long, E. H. Neilsen, Jr., A. Nitta, S. A. Snedden, and W. Voges. A Survey of $z_{\text{c}}5.7$ Quasars in the Sloan Digital Sky Survey. IV. Discovery of Seven Additional Quasars. *AJ*, 131:1203–1209, March 2006. .
- GB Field. Excitation of the hydrogen 21-cm line. *Proceedings of the Institute Radio Engineers*, 46:240–250, 1958. .
- S. R. Furlanetto, S. P. Oh, and F. H. Briggs. Cosmology at low frequencies: The 21 cm transition and the high-redshift Universe. *Phys. Rep.*, 433:181–301, October 2006. .
- D. Hooper and L.-T. Wang. Possible evidence for axino dark matter in the galactic bulge. *Phys. Rev. D*, 70(6):063506–+, September 2004. .
- M. Kuhlen, P. Madau, and R. Montgomery. The Spin Temperature and 21 cm Brightness of the Intergalactic Medium in the Pre-Reionization era. *ApJ*, 637:L1–L4, January 2006. .
- H. Liszt. The spin temperature of warm interstellar H I. *A&A*, 371:698–707, May 2001. .
- P. Madau, A. Meiksin, and M. J. Rees. 21 Centimeter Tomography of the Intergalactic Medium at High Redshift. *ApJ*, 475:429–+, February 1997. .
- M. Mapelli and A. Ferrara. Background radiation from sterile neutrino decay and reionization. *MNRAS*, 364:2–12, November 2005. .
- M. Mapelli, A. Ferrara, and E. Pierpaoli. Impact of dark matter decays and annihilations on reionization. *MNRAS*, 369:1719–1724, July 2006. .
- Z. Myers and A. Nusser. Neutralino annihilations and the gas temperature in the dark ages. *MNRAS*, 384:727–732, February 2008. .
- D. E. Osterbrock. *Astrophysics of gaseous nebulae and active galactic nuclei*. Research supported by the University of California, John Simon Guggenheim Memorial Foundation, University of Minnesota, et al. Mill Valley, CA, University Science Books, 1989, 422 p., 1989. .
- N. Padmanabhan and D. P. Finkbeiner. Detecting dark matter annihilation with CMB polarization: Signatures and experimental prospects. *Phys. Rev. D*, 72(2):023508–+, July 2005. .
- R. M. Pengelly. Recombination spectra, I. *MNRAS*, 127:145–+, 1964. .
- E. Ripamonti, M. Mapelli, and A. Ferrara. Intergalactic medium heating by dark matter. *MNRAS*, 374:1067–1077, January 2007. .
- G. B. Rybicki and A. P. Lightman. *Radiative processes in astrophysics*. New York, Wiley-Interscience, 1979. 393 p., 1979. .
- S. Seager, D. D. Sasselov, and D. Scott. A New Calculation of the Recombination Epoch. *ApJ*, 523:L1–L5, September 1999. .
- J. M. Shull and M. E. van Steenberg. X-ray secondary heating and ionization in quasar emission-line clouds. *ApJ*, 298:268–274, November 1985. .
- F. J. Smith. Hydrogen atom spin-change collisions. *Planet. Space Sci.*, 14:929–+, October 1966. .

- M. Valdés, A. Ferrara, M. Mapelli, and E. Ripamonti. Constraining dark matter through 21-cm observations. *MNRAS*, 377:245–252, May 2007. .
- C. R. Watson, J. F. Beacom, H. Yüksel, and T. P. Walker. Direct x-ray constraints on sterile neutrino warm dark matter. *Phys. Rev. D*, 74(3):033009–+, August 2006. .
- A. A. Zdziarski and R. Svensson. Absorption of X-rays and gamma rays at cosmological distances. *ApJ*, 344:551–566, September 1989. .
- B. Zygelman. Hyperfine Level-changing Collisions of Hydrogen Atoms and Tomography of the Dark Age Universe. *ApJ*, 622:1356–1362, April 2005. .

5. Appendix

This appendix contains all figures created with my code. The cases deemed most interesting (based on their effects on the IGM) have been selected for display in section 3. The first set of figures shown have an energy spectrum with a power law index of 1. Following that are figures with a mono-energetic spectrum. Then the figures with peculiar energy spectra follow. Figures of the energy absorbed fractions and the differential brightness temperatures are displayed last.

Because the lines shown in the figures for the thermal history of the universe represent the same physical quantities we refer to the preceding section for an explanation of these. Consequently, they will not be explained below.

5.1. Figures with $dn/dE = E^{-1}$

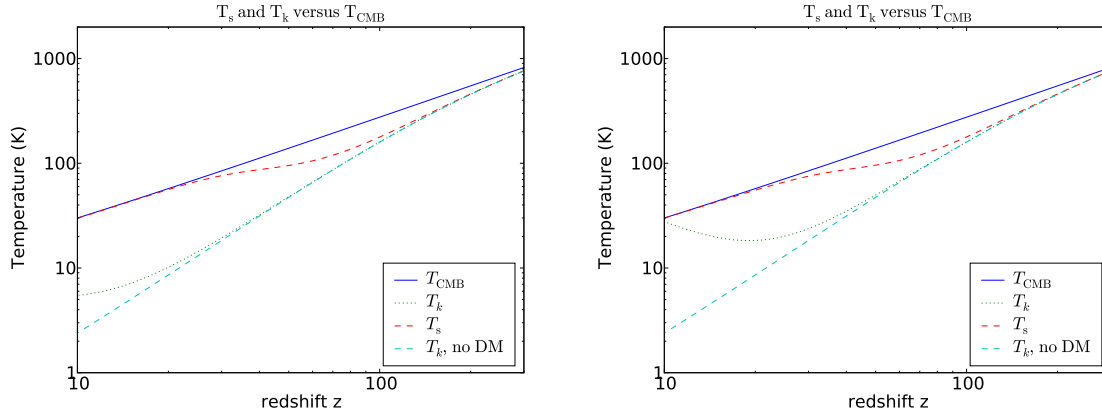


Fig. 11: Left panel: T_s (red dashed line) and T_k with (without) DM influence, green dotted line (light-blue dashed line), T_{CMB} (solid blue line) as function of redshift z for 25 keV decaying SN into 10% photons with an energy spectrum $dn/dE = E^{-1}$. Right panel: T_s (red dashed line) and T_k with (without) DM influence, green dotted line (light-blue dashed line), T_{CMB} (solid blue line) as function of redshift z for 25 keV decaying SN into 10% electrons with an energy spectrum $dn/dE = E^{-1}$.

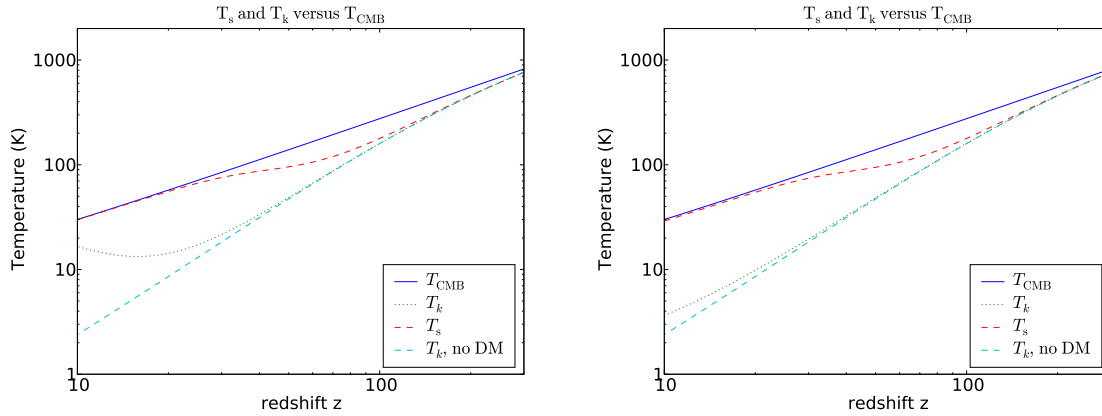


Fig. 12: Left panel: T_s (red dashed line) and T_k with (without) DM influence, green dotted line (light-blue dashed line), T_{CMB} (solid blue line) as function of redshift z for 25 keV decaying SN into 5% photons & 5% electrons with an energy spectrum $dn/dE = E^{-1}$. Right panel: T_s (red dashed line) and T_k with (without) DM influence, green dotted line (light-blue dashed line), T_{CMB} (solid blue line) as function of redshift z for 10 MeV decaying LDM into 10% photons with an energy spectrum $dn/dE = E^{-1}$.

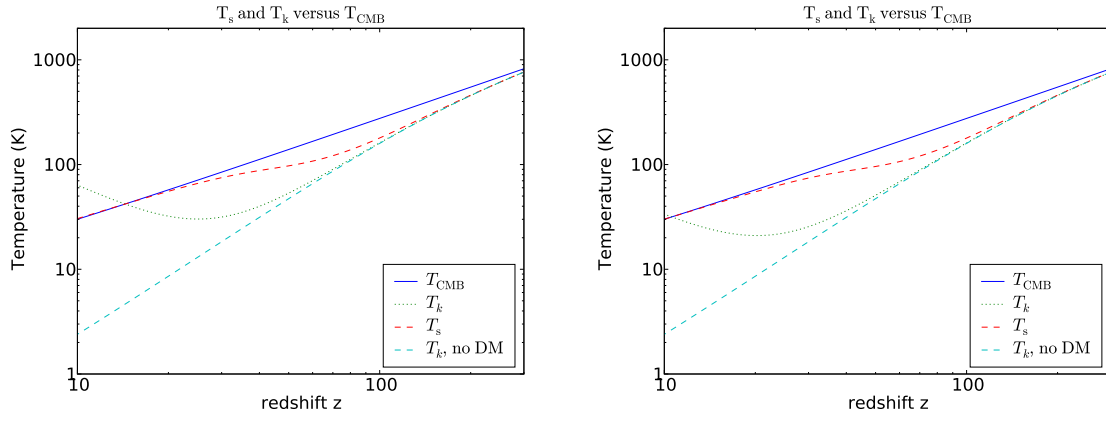


Fig. 13: Left panel: T_s (red dashed line) and T_k with (without) DM influence, green dotted line (light-blue dashed line), T_{CMB} (solid blue line) as function of redshift z for 10 MeV decaying LDM into 10% electrons with an energy spectrum $dn/dE = E^{-1}$. Right panel: T_s (red dashed line) and T_k with (without) DM influence, green dotted line (light-blue dashed line), T_{CMB} (solid blue line) as function of redshift z for 10 MeV decaying LDM into 5% photons & 5% electrons with an energy spectrum $dn/dE = E^{-1}$.

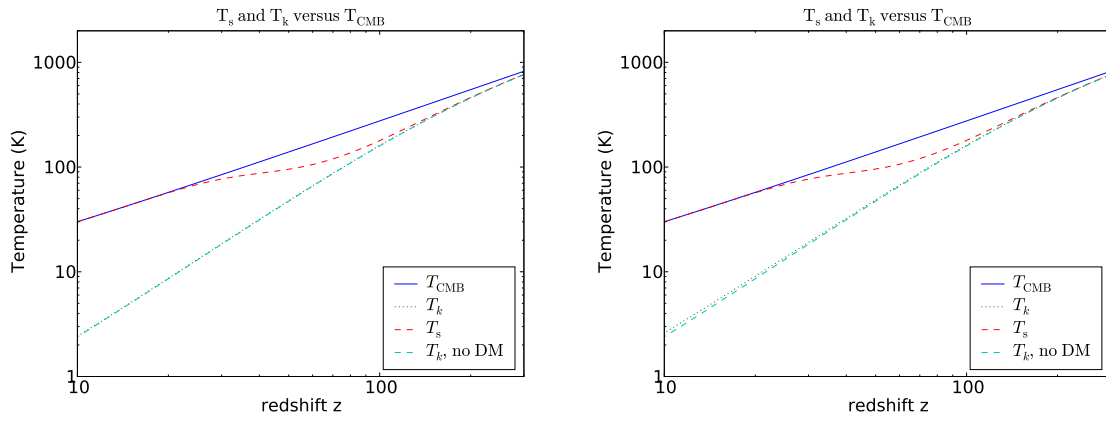


Fig. 14: Left panel: T_s (red dashed line) and T_k with (without) DM influence, green dotted line (light-blue dashed line), T_{CMB} (solid blue line) as function of redshift z for 10 MeV annihilating LDM into 10% photons with an energy spectrum $dn/dE = E^{-1}$. Right panel: T_s (red dashed line) and T_k with (without) DM influence, green dotted line (light-blue dashed line), T_{CMB} (solid blue line) as function of redshift z for 10 MeV annihilating LDM into 10% electrons with an energy spectrum $dn/dE = E^{-1}$.

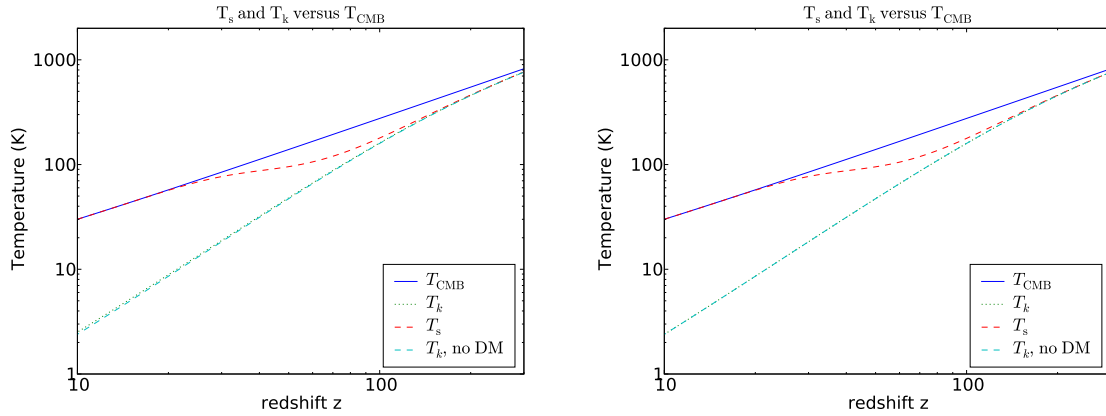


Fig. 15: Left panel: T_s (red dashed line) and T_k with (without) DM influence, green dotted line (light-blue dashed line), T_{CMB} (solid blue line) as function of redshift z for 10 MeV annihilating LDM into 5% photons & 5% electrons with an energy spectrum $dn/dE = E^{-1}$. Right panel: T_s (red dashed line) and T_k with (without) DM influence, green dotted line (light-blue dashed line), T_{CMB} (solid blue line) as function of redshift z for 50 GeV annihilating XDM into 10% photons with an energy spectrum $dn/dE = E^{-1}$.

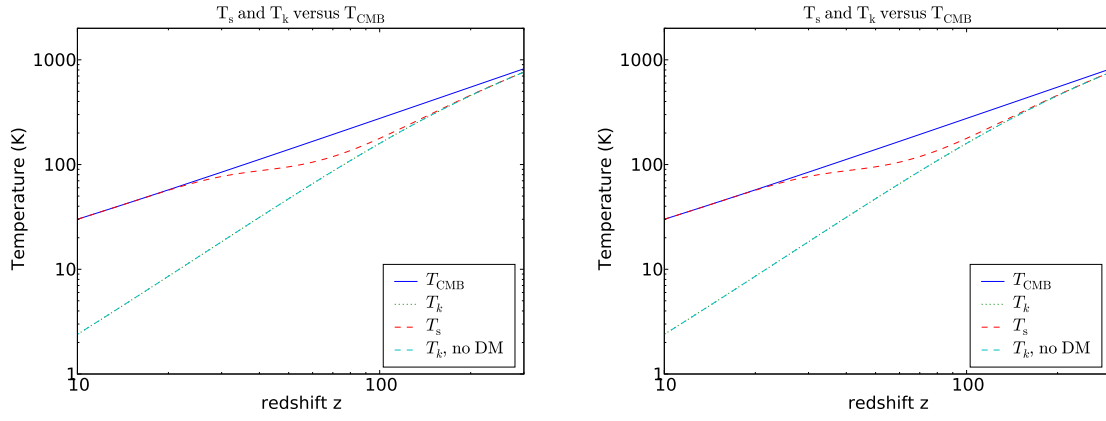


Fig. 16: Left panel: T_s (red dashed line) and T_k with (without) DM influence, green dotted line (light-blue dashed line), T_{CMB} (solid blue line) as function of redshift z for 100 GeV annihilating neutralinos into 10% photons with an energy spectrum $dn/dE = E^{-1}$. Right panel: T_s (red dashed line) and T_k with (without) DM influence, green dotted line (light-blue dashed line), T_{CMB} (solid blue line) as function of redshift z for 100 GeV annihilating neutralinos into electrons with an energy spectrum $dn/dE = E^{-2}$, using the Myers and Nusser (2008) data, 10% of energy into electrons.

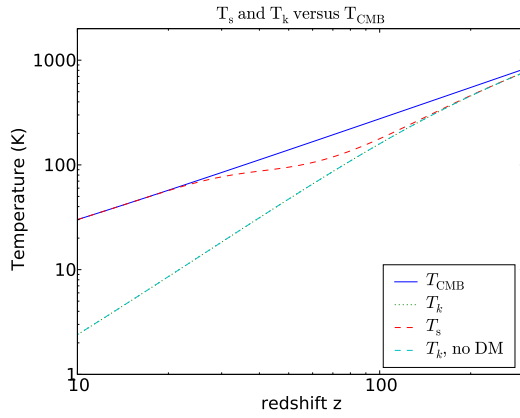


Fig. 17: Left panel: T_s (red dashed line) and T_k with (without) DM influence, green dotted line (light-blue dashed line), T_{CMB} (solid blue line) as function of redshift z for 100 GeV annihilating neutralinos into 5% photons & 5% electrons with an energy spectrum $dn/dE = E^{-1}$.

5.2. Figures with a mono-energetic energy spectrum

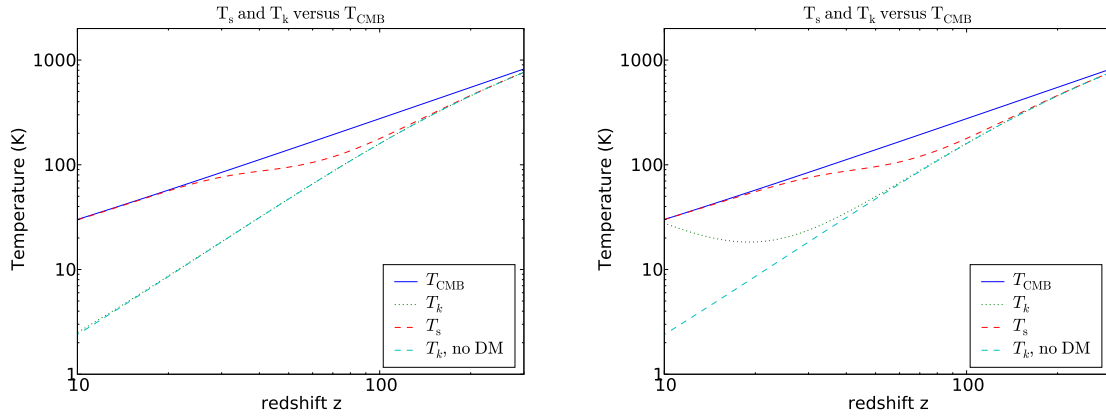


Fig. 18: Left panel: T_s (red dashed line) and T_k with (without) DM influence, green dotted line (light-blue dashed line), T_{CMB} (solid blue line) as function of redshift z for 25 keV decaying LDM into 10% photons with a mono-energetic energy spectrum. Right panel: T_s (red dashed line) and T_k with (without) DM influence, green dotted line (light-blue dashed line), T_{CMB} (solid blue line) as function of redshift z for 25 keV decaying LDM into 10% electrons with a mono-energetic energy spectrum.

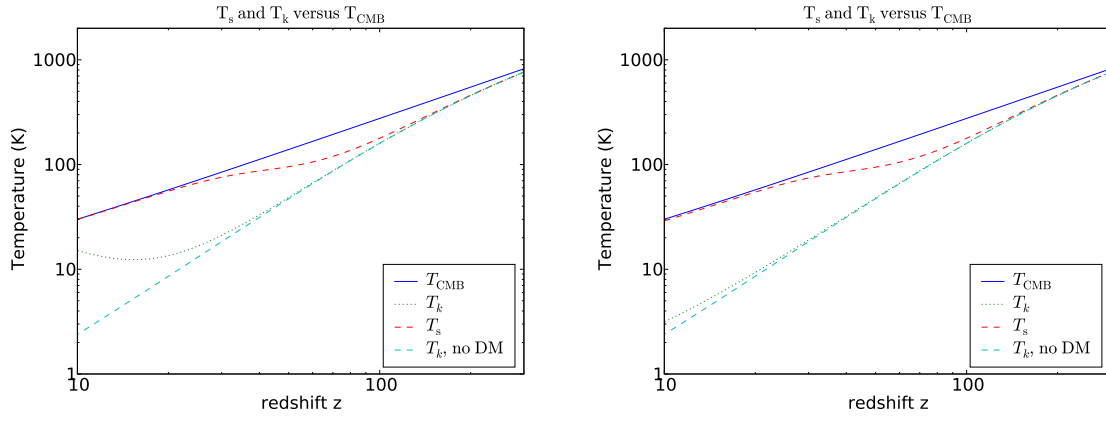


Fig. 19: Left panel: T_s (red dashed line) and T_k with (without) DM influence, green dotted line (light-blue dashed line), T_{CMB} (solid blue line) as function of redshift z for 25 keV decaying LDM into 5% photons & 5% electrons with a mono-energetic energy spectrum. Right panel: T_s (red dashed line) and T_k with (without) DM influence, green dotted line (light-blue dashed line), T_{CMB} (solid blue line) as function of redshift z for 10 MeV decaying LDM into 10% photons with a mono-energetic energy spectrum.

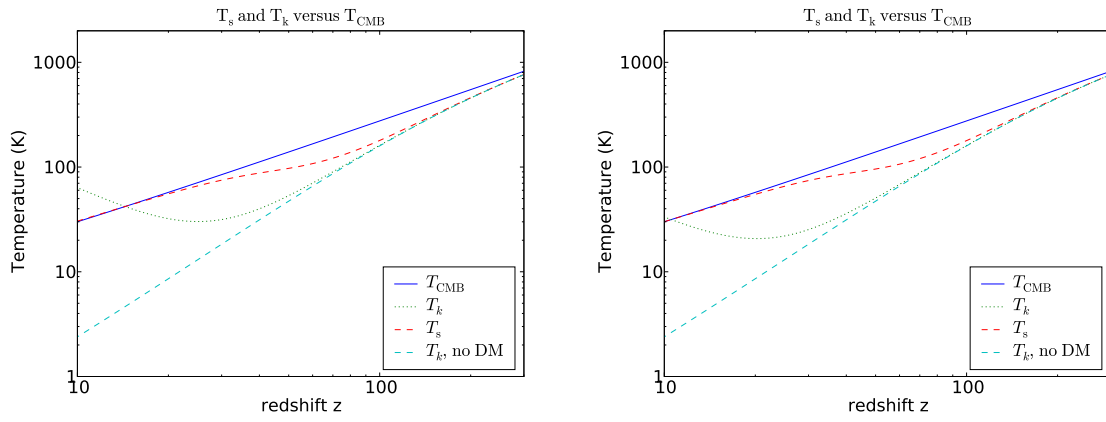


Fig. 20: Left panel: T_s (red dashed line) and T_k with (without) DM influence, green dotted line (light-blue dashed line), T_{CMB} (solid blue line) as function of redshift z for 10 MeV decaying LDM into 10% electrons with a mono-energetic energy spectrum. Right panel: T_s (red dashed line) and T_k with (without) DM influence, green dotted line (light-blue dashed line), T_{CMB} (solid blue line) as function of redshift z for 10 MeV decaying LDM into 5% photons & 5% electrons with a mono-energetic energy spectrum.

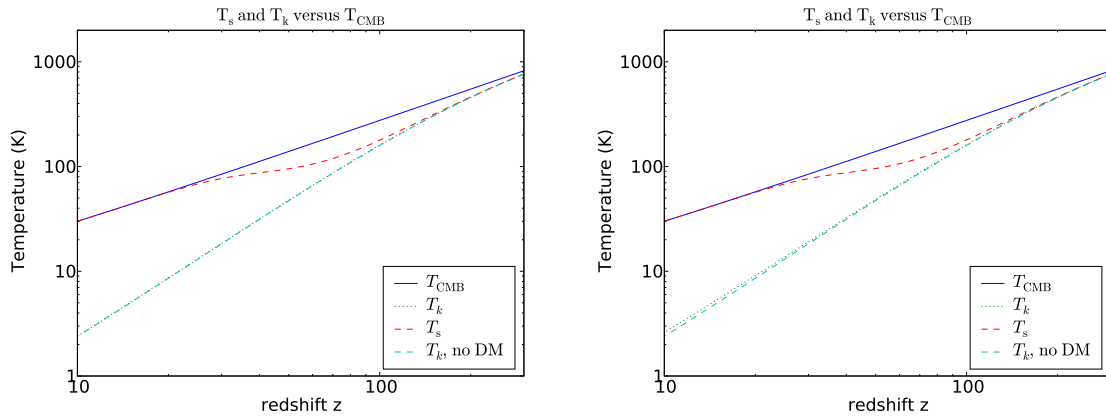


Fig. 21: Left panel: T_s (red dashed line) and T_k with (without) DM influence, green dotted line (light-blue dashed line), T_{CMB} (solid blue line) as function of redshift z for 10 MeV annihilating LDM into 10% photons with a mono-energetic energy spectrum. Right panel: T_s (red dashed line) and T_k with (without) DM influence, green dotted line (light-blue dashed line), T_{CMB} (solid blue line) as function of redshift z for 10 MeV annihilating LDM into 10% electrons with a mono-energetic energy spectrum.

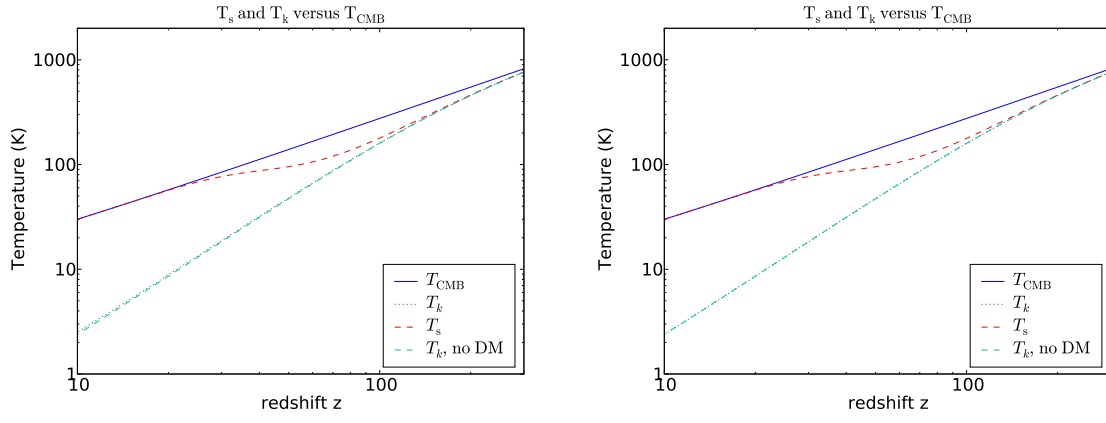


Fig. 22: Left panel: T_s (red dashed line) and T_k with (without) DM influence, green dotted line (light-blue dashed line), T_{CMB} (solid blue line) as function of redshift z for 10 MeV annihilating LDM into 5% photons & 5% electrons with a mono-energetic energy spectrum. Right panel: T_s (red dashed line) and T_k with (without) DM influence, green dotted line (light-blue dashed line), T_{CMB} (solid blue line) as function of redshift z for 50 GeV annihilating XDM into 10% photons with a mono-energetic energy spectrum.

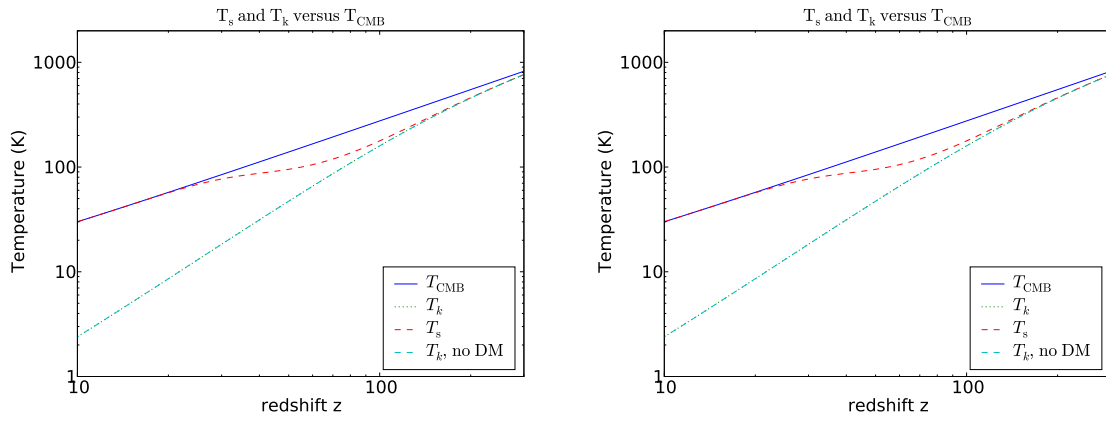


Fig. 23: Left panel: T_s (red dashed line) and T_k with (without) DM influence, green dotted line (light-blue dashed line), T_{CMB} (solid blue line) as function of redshift z for 50 GeV annihilating XDM into 10% photons with a mono-energetic energy spectrum. Right panel: T_s (red dashed line) and T_k with (without) DM influence, green dotted line (light-blue dashed line), T_{CMB} (solid blue line) as function of redshift z for 100 GeV annihilating neutralinos into 10% photons with a mono-energetic energy spectrum.

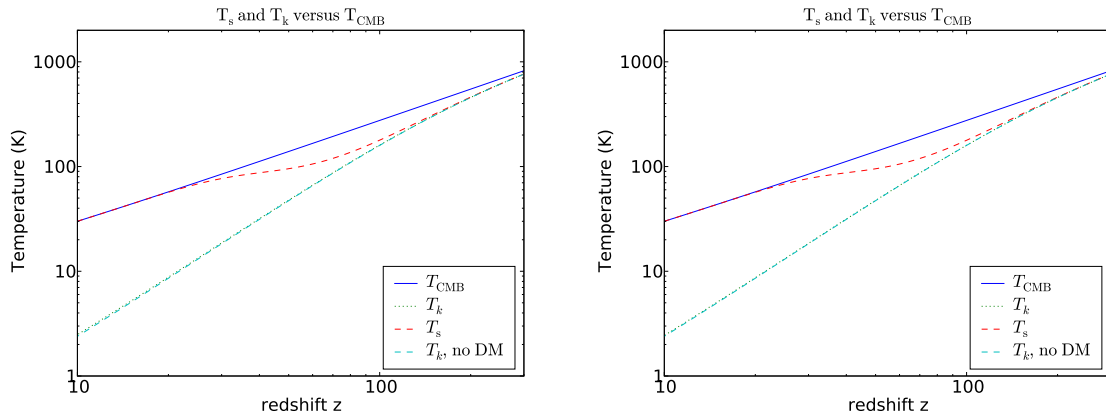


Fig. 24: Left panel: T_s (red dashed line) and T_k with (without) DM influence, green dotted line (light-blue dashed line), T_{CMB} (solid blue line) as function of redshift z for 100 GeV annihilating neutralinos into electrons with a mono-energetic energy spectrum, using the Myers and Nusser (2008) data (10% of energy into electrons). Right panel: T_s (red dashed line) and T_k with (without) DM influence, green dotted line (light-blue dashed line), T_{CMB} (solid blue line) as function of redshift z for 100 GeV annihilating neutralinos into 5% photons & 5% electrons with a mono-energetic energy spectrum.

5.3. Other energy spectra

MDM has an $E^{-2.64}$ energy spectrum and energy range 20-60 GeV.

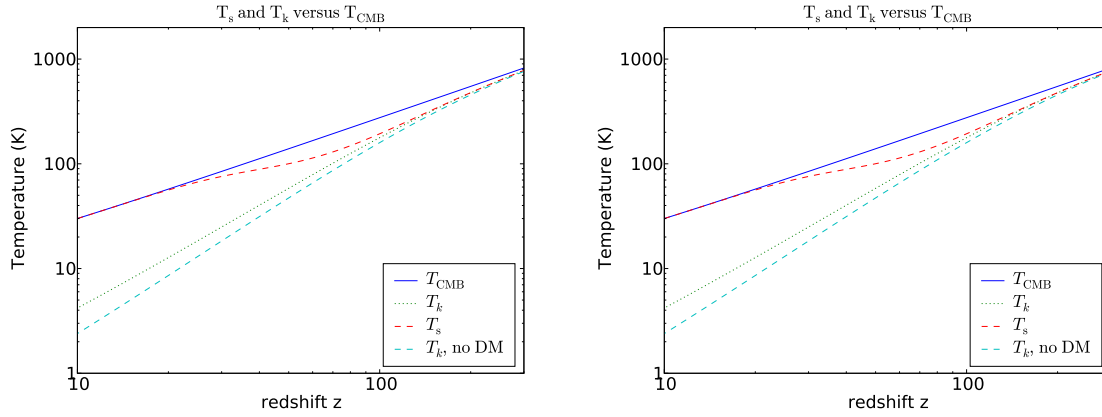


Fig. 25: Left panel: T_s (red dashed line) and T_k with (without) DM influence, green dotted line (light-blue dashed line), T_{CMB} (solid blue line) as function of redshift z for 20 GeV annihilating MDM into 10% photons with an energy spectrum $dn/dE = E^{-2.64}$. Right panel: T_s (red dashed line) and T_k with (without) DM influence, green dotted line (light-blue dashed line), T_{CMB} (solid blue line) as function of redshift z for 20 GeV annihilating MDM into 10% electrons with an energy spectrum $dn/dE = E^{-2.64}$.

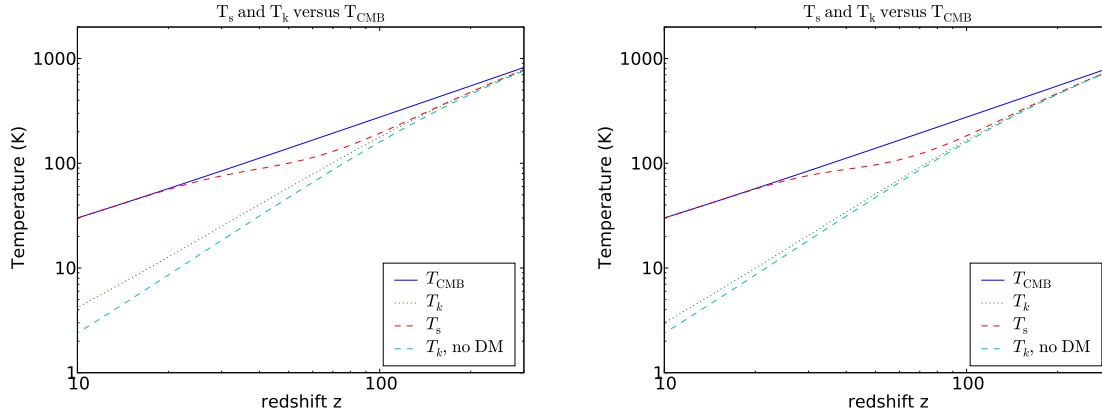


Fig. 26: Left panel: T_s (red dashed line) and T_k with (without) DM influence, green dotted line (light-blue dashed line), T_{CMB} (solid blue line) as function of redshift z for 20 GeV annihilating MDM into 5% photons & 5% electrons with an energy spectrum $dn/dE = E^{-2.64}$. Right panel: T_s (red dashed line) and T_k with (without) DM influence, green dotted line (light-blue dashed line), T_{CMB} (solid blue line) as function of redshift z for 60 GeV annihilating MDM into 10% photons with an energy spectrum $dn/dE = E^{-2.64}$.

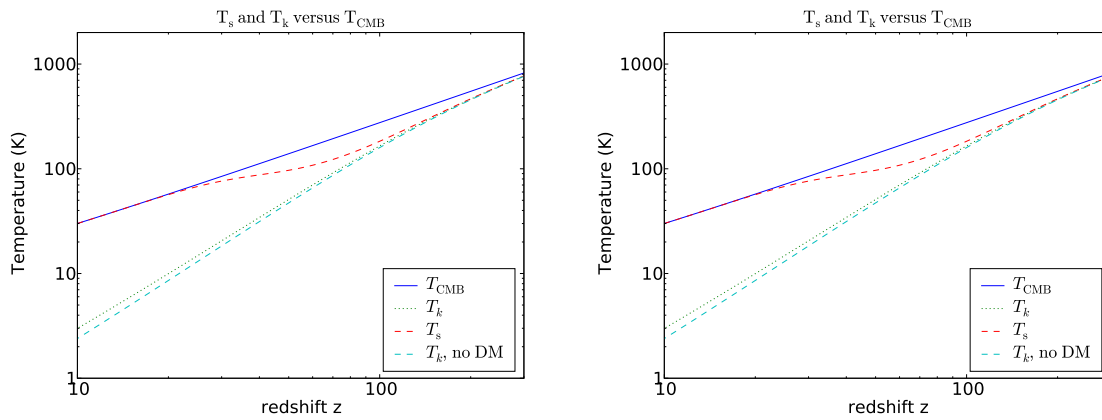


Fig. 27: Left panel: T_s (red dashed line) and T_k with (without) DM influence, green dotted line (light-blue dashed line), T_{CMB} (solid blue line) as function of redshift z for 60 GeV annihilating MDM into 10% electrons with an energy spectrum $dn/dE = E^{-2.64}$. Right panel: T_s (red dashed line) and T_k with (without) DM influence, green dotted line (light-blue dashed line), T_{CMB} (solid blue line) as function of redshift z for 60 GeV annihilating MDM into 5% photons & 5% electrons with an energy spectrum $dn/dE = E^{-2.64}$.

5.4. Differential brightness temperatures

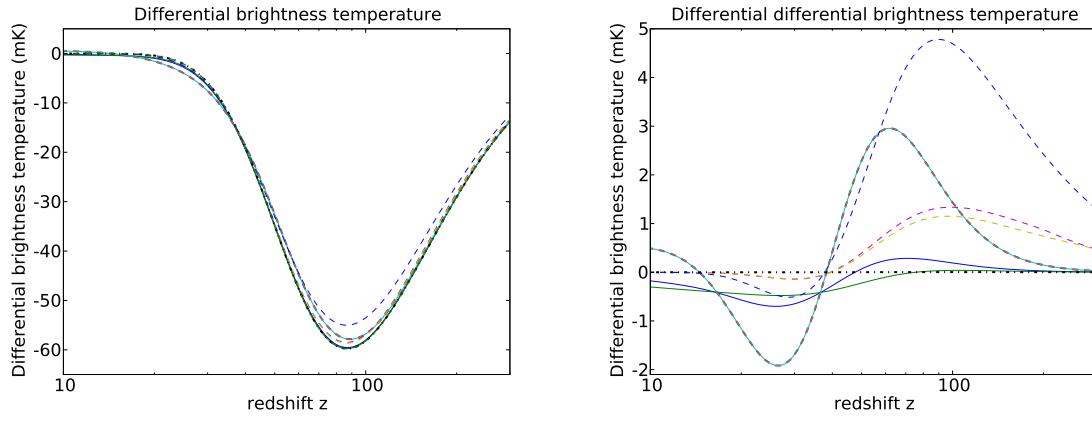


Fig. 28: Left panel: shows the differential brightness temperatures. Right panel: shows the differential differential brightness temperatures (with respect to the non-DM thermal history). For both panels, the dashed green line corresponds to the standard case without DM influence, solid blue line (solid green line) corresponds to 25 keV decaying sterile neutrinos with (without) an energy spectrum. Dashed red line (solid light-blue line) corresponds to 10 MeV decaying LDM with (without) an energy spectrum. Dashed purple (dashed yellow) line corresponds to 10 MeV annihilating LDM. Dash-dotted black line corresponds to 100 GeV annihilating neutralinos with an energy spectrum, dashed green line corresponds to 60 GeV annihilating MDM with an energy spectrum.

5.5. Absorbed fractions

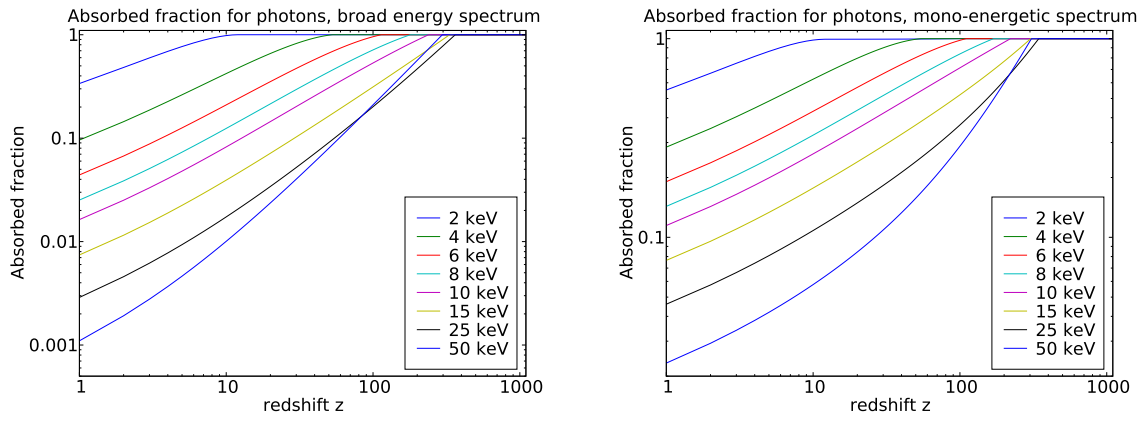


Fig. 29: Left panel: Absorbed fraction z for photons of several energies with powerlaw index 1. Right panel: Absorbed fraction for photons for several energies with an mono-energetic energy spectrum.

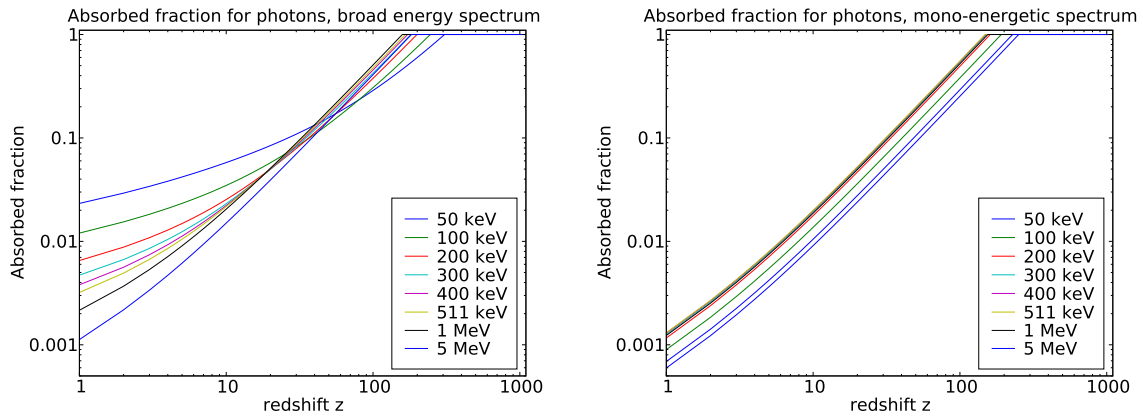


Fig. 30: Left panel: Absorbed fraction for photons of higher energies with powerlaw index 1. Right panel: Absorbed fraction for photons of higher energies with mono-energetic energy spectrum.